

SEL-67-071

A RADAR INVESTIGATION OF THE SOLAR CORONA

by

John E. Ohlson

August 1967

Scientific Report No. 21

Prepared under

National Aeronautics and Space Administration
Research Grant No. Nsg-377

and

Scientific Report No. 1

Prepared under

National Science Foundation Grant No. GP-2711

Radioscience Laboratory
Stanford Electronics Laboratories
Stanford University Stanford, California

PRECEDING PAGE BLANK NOT FILMED.

ABSTRACT

During the summers of 1963, 1964, and 1965, over 200 attempts were made at Stanford University to obtain radar reflections from the solar corona. A frequency near 25 MHz was used with a 300 kW transmitter and an antenna of 25 dB gain. The signal was produced by transmitting a sine wave on one or the other of two distinct frequencies for 4 sec at a time. The spacing of the two frequencies was 16, 40, and 50 kHz for successive years. For unambiguous range resolution, a special coding scheme (maximum-length sequence) was employed to determine the transmitter frequency for each 4 sec interval. Transmission was for the approximate time needed for the radar signal to travel to the sun and return to earth (about 1000 sec). Reception followed the cessation of transmission and continued for the expected duration of the reflected signal with receivers tuned to the two transmitted frequencies. Signal processing included square-law detection and extensive use of a digital computer to search the received data for the transmitted signal, using the technique of crosscorrelation. A dual-frequency system was used, for it efficiently reduces the corruptive effects of nonstationary noise from the sun and our galaxy.

Positive indications of echo returns were not obtained for any of the individual runs, so groups of runs were weighted and summed according to various criteria in order to improve the detection capability. These criteria

included segregation and weighting by year, noise level, sunspot number, and the daily values of solar radar cross-section measured at 38 MHz by the M.I.T. Astronomical Radar Station near El Campo, Texas. These summations indicated that the echoes were too weak for reliable detection.

Extensive evidence is given that the radar system functioned properly during the experiments. This was demonstrated by use of the principal system components in extensive lunar radar work, by test runs involving the entire system, and by reduction of M.I.T. solar echo data with the same results as they obtained. On this basis, a strong conclusion may be drawn concerning the radar cross section of the sun during this period. It is shown that a radar cross section of twice the cross-sectional area of the visual disk would produce a readily detectable signal. Thus, for several months during 1963-1965, the radar cross section of the sun at 25 MHz was less than two units of disk area. This becomes very interesting when compared to the 1959 Stanford results at the same frequency. In 1959, six separate measurements with positive results indicated a radar cross section of about 80 times the visual disk area. Since 1959 was near a maximum of the 11-year sunspot cycle and the present data centered around the minimum of 1964, there appears to be a strong correlation between the sun's radar cross section at 25 MHz and its general activity as indexed by the sunspot number. A large decrease of the average radar cross section

was observed at 38 MHz by the M.I.T. group from 1961 to 1965. This lends credence to the present conclusion. In addition, the present results show (at least during sunspot minimum) that the radar cross section at 25 MHz is not significantly greater than at 38 MHz, as has been variously suggested.

An analysis of the entire system is made, accounting for both time and frequency spread of the returned signal. An analysis is also made of the effect of fluctuations in the returned signal caused by the time-varying reflectivity of the corona and to Faraday fading in the ionosphere and corona.

CONTENTS

<u>Chapter</u>	<u>Page</u>
I. Introduction	1
II. Radar Characteristics of the Sun	4
III. The Stanford Solar Radar	7
IV. System Analysis	14
A. Time Spreading Effects	26
B. Amplitude Fluctuations of the Received Signal	31
V. System Validation	44
VI. Experimental Results	53
A. Weighted Summations of Data Runs	60
B. Comparison with Other Experiments	68
VII. Conclusions	71
A. Summary and Conclusions	71
B. Suggestions for Future Work	72
APPENDIX. Signal Processor Analysis	74
BIBLIOGRAPHY	84

ILLUSTRATIONS

<u>Figure</u>		<u>Page</u>
1.	Stanford solar radar block diagram	7
2.	Signal processor block diagram	10
3.	Simplified system	11
4.	A possible echo spectrum	16
5.	A possible power impulse response	16
6.	Signal autocorrelation	18
7.	Receiver model	19
8.	A possible set of power spectra for the random carriers	22
9.	Input and output power spectra for square-law detection	29
10.	A possible fading autocorrelation function . .	35
11.	A triangular form of the fading auto- correlation function	36
12.	Fractional measurement error as a function of fading time and signal length	39
13.	Test signal output correlation	49
14.	Typical data from a run in the 1965 series (tape 589-2)	50
15.	Correlation outputs from El Campo tape EC-43 .	52
16.	Correlation outputs from El Campo tape EC-44 .	52
17.	Estimated 25 MHz frequency spread based upon El Campo results at 38 MHz	54
18.	Typical 1963 correlation output - tape 283-2 .	58
19.	Typical 1964 correlation output - tape 499-1 .	59
20.	Typical 1965 correlation output - tape 595-1 .	59
21.	1963 summation of 61 runs	63

ILLUSTRATIONS (Cont)

<u>Figure</u>	<u>Page</u>
22. 1964 summation of 128 runs	63
23. 1965 summation of 38 runs	64
24. Total summation of 227 runs	64
25. El Campo weighting and summation of 28 runs from 1963	66
26. El Campo weighting and summation of 62 runs from 1964	66
27. El Campo weighting and summation of 32 runs from 1965	67
28. El Campo weighting and summation of 122 runs for 1963, 1964, 1965	67
29. Comparison of radar cross section measurements	69

TABLE

Number

1. Summary of operating frequencies	9
---	---

ACKNOWLEDGMENT

The author wishes to express his appreciation for the encouragement and advice given by the supervisors of this research, Professors A. M. Peterson and V. R. Eshleman. Thanks must also be given to H. T. Howard, who directed the experiments, and to J. C. James of the M.I.T. Astronomical Observatory, El Campo, Texas, who very kindly provided data on the solar radar results of that facility.

The research reported in this paper was supported by the National Science Foundation and the National Aeronautics and Space Administration.

CHAPTER I
INTRODUCTION

In 1959 the first successful attempts to obtain radar echoes from the sun were made at Stanford University [Eshleman et al, 1960; Barthle, 1960]. The frequency used was near 26 MHz and positive echo indications were received for six attempts on five separate days. Since 1961 the Radar Astronomical Station of the Massachusetts Institute of Technology Center for Space Research located near El Campo, Texas, has intensively studied the radar properties of the sun near 38 MHz [Abel et al, 1961 and 1962; Chisholm et al, 1964; James, 1964 and 1966]. Over 1000 runs have been made and extensive analysis has provided much information. Two facts stand out: (1) The average radar cross section of the sun measured at 38 MHz has been smaller than the apparent cross section seen by the 1959 Stanford group at 26 MHz; and (2) M.I.T. experienced a large decrease of cross section as the sunspot number decreased between 1961 and 1964-1965.

A small number of runs were made during the summer of 1966 at the Arecibo Ionospheric Observatory facility in Puerto Rico. A frequency of 40 MHz was used, and cross section values substantially in agreement with the El Campo measurements were obtained [Dyce].

At Stanford in 1962, attempts to detect the sun were begun with a different and more sensitive system than was used in the 1959 experiments. Equipment problems (and/or

lack of sufficient signal) prevented any signal detection in that series of experiments. By the summer of 1963, the system was fully ready and extensive data were taken then, and additionally in 1964 and 1965.

The purpose of the experiments was to obtain information on several measurable radar parameters at 25 MHz and to compare them with the M.I.T. results at 38 MHz and the earlier Stanford work at 26 MHz. The radar cross section of the sun and its time variance was the first parameter in importance. Second was to be the measurement of total round-trip travel time which would then give a measure of the depth of penetration of the signal into the corona. Coupled with these measurements would be an indication of the time spreading of the returned signal due to the "soft" coronal target. This would provide information on the distribution of electrons within the corona. In addition, a spectral analysis of the returned signal would give information as to the gross motion and turbulence of the corona.

The details, analysis, and results of the Stanford solar radar system used in 1963, 1964, and 1965 are presented in this report. A model for the reflected signal is established which incorporates the time and frequency spreading introduced by the corona. The optimum detection scheme for a soft target with certain restrictions upon the target's scattering function is then established. Two statistical models of the fading phenomenon due to Faraday rotation are proposed and evaluated.

In addition, a quasi-stationary model for the time-varying reflectivity of the corona is proposed. The effects of fading and a variable coronal reflectivity upon the measurement of the solar cross section are then evaluated and discussed.

CHAPTER II

RADAR CHARACTERISTICS OF THE SUN

As opposed to airplanes, buildings, and planets which possess physically stable features and are called "hard" targets, the sun presents a "soft" target. Optically, the sun appears to be restricted to the disk which subtends one-half degree of arc from the earth. This is known as the photosphere, but the region called the corona, which is essentially fully ionized hydrogen, actually extends many solar radii outward from the visual sun. It is in this region that radar signals are reflected. That this region exists can be seen from examination of any photograph of the sun taken during a solar eclipse. This region apparently possesses turbulence as well as gross outward motion (solar wind). The electron density falls with distance away from the sun. Within the coronal region, an electromagnetic wave may propagate, providing the index of refraction is greater than zero. If we assume a negligible magnetic field, this quantity, n , is given by

$$n^2 = 1 - \frac{Ne^2}{\epsilon_0 m(\omega^2 + \nu^2)} \quad (1)$$

where N is the electron density, ν is the collision frequency, ω is the radian frequency, e and m represent the charge and mass of the electron, and ϵ_0 is free space permittivity. When an electromagnetic wave reaches a surface

of $n = 0$, it can no longer propagate and is therefore reflected. The corona is not symmetric and varies with time, therefore the reflecting surface presents an irregular reflector of varying shape. The resultant returned radar signal is thus smeared in time due to reflection from various depths in the corona. It is also smeared in frequency due to coronal turbulence which produces doppler spreading.

Attenuation of the signal due to absorption, as well as group path time delay, will also occur. Since a higher frequency signal will penetrate further into the corona before being reflected, the attenuation will be larger as well. However, high antenna gains are more readily obtained as the wavelength becomes smaller. Overall quantitative considerations [Kerr, 1952; Bass and Braude, 1957] have indicated that a frequency in the 20 to 50 MHz range is probably optimum for radar detection, with the lower limit being imposed by the earth's ionosphere. A number of measurements were made at the Jicamarca Radar Observatory in Peru in 1963 and 1964 at 50 MHz [Klemperer]. No echoes were detected, although the system sensitivity was such that if the radar cross section were comparable at 38 and 50 MHz, positive results would have been obtained. This indicates that 50 MHz is probably above the optimum frequency range.

Because of the large time and frequency spreading of the reflected signal in the corona, normal radar techniques for hard targets are quite impractical. The frequency spread

requires that a wide bandwidth be used, but this then permits a great amount of noise to enter the system. Because of the time spreading, coherent signal detection cannot be achieved and detection can only be performed on the basis of received energy. However, it is precisely because of these effects that the nature of the sun may be investigated. Because of the dynamic nature of the sun, it certainly is the most interesting target presently capable of being studied by earth-based radar.

CHAPTER III
THE STANFORD SOLAR RADAR

Figure 1 is a block diagram of the Stanford solar radar. The antenna is described elsewhere [Howard, 1965]; but briefly, it is a phased array of 48 log-periodic elements arranged in two parallel 1150 ft rows of 24 elements each.

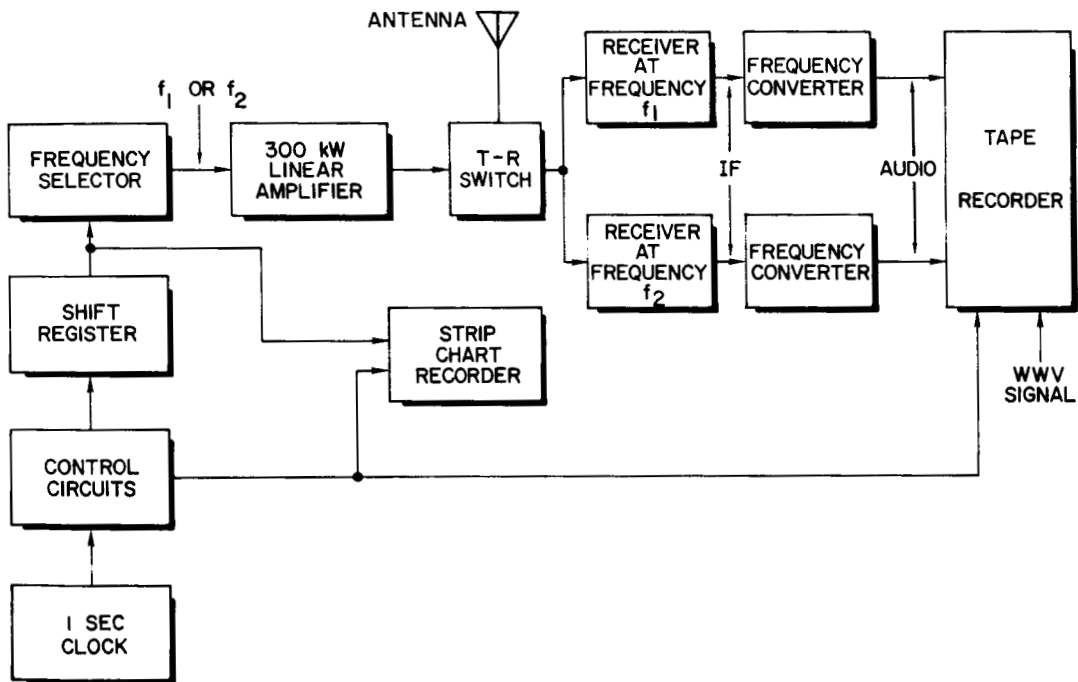


Fig. 1. STANFORD SOLAR RADAR BLOCK DIAGRAM.

The antenna was designed for radar astronomy purposes and has a fan beam with a thickness of approximately 2° north to south and a width of about 30° east to west. The measured gain is 25.3 dB.

The transmitter is a linear amplifier capable of 300 kW

average power output. The transmitted signal is a frequency-shift-keyed sinusoid with basic pulse length of 4 sec. The frequency was near 25 MHz for all three years, while the frequency shift was 16 kHz, 40 kHz, and 50 kHz for 1963, 1964, and 1965, respectively. The keying is derived from a seven-stage feedback shift register [Golomb, 1964]. A shift register of n stages with proper feedback produces a periodic binary sequence of period $2^n - 1$. Thus the basic sequence length is 127. It is repeated nearly twice to provide a total signal length of about 1000 sec, which is the nominal round-trip travel time for signals reflected from the sun. (Chapter IV will discuss the signal in more detail.)

The keying sequence is recorded on a strip chart for later verification. The control circuits provide the necessary timing and counting to guarantee timing knowledge in the reduction of the recorded data. The tape recorder was turned on 30 sec before the transmit sequence ended. After the transmitter was turned off and the receivers were connected, the 1 sec clock was recorded on the strip chart and magnetic tape. This began at an integral number of seconds from transmit beginning and continued throughout the reception period.

The R-390 receivers (one for each transmitted frequency) were tuned slightly higher than the transmitted frequencies in anticipation of doppler shift. The receiver bandwidths were nominally 16 kHz. The receivers' automatic gain controls were left off and the intermediate frequency signal was

translated down to the audio range and recorded. Table 1 lists the various frequencies involved. The tape recorder center frequency corresponds to that frequency to which the IF center frequency (455 kHz) is shifted. The tape recorder zero-doppler frequency is the frequency where returned signal would be found if no doppler spread or shift were experienced.

TABLE 1. SUMMARY OF OPERATING FREQUENCIES

Year	Transmitter Frequencies (MHz)	Receiver Frequencies (MHz)	Tape Recorder Center Frequency (kHz)	Tape Recorder Zero-Doppler Frequency (kHz)
1963	24.900	24.901	12.4	11.4
	24.916	24.917		
1964	24.901	24.903	12.4	10.4
	24.941	24.943		
1965	24.825	24.827	9.0	7.0
	24.875	24.877		

A block diagram of the signal processor is shown in Fig. 2. The signal passes through a filter to eliminate noise outside the data bandwidth (principally 60 Hz and tape noise); it is limited to eliminate impulsive noise and interference, and then squared to obtain the power. The power is then integrated for 1 sec periods and sampled. The voltage-to-frequency converter produces a pulse train whose frequency

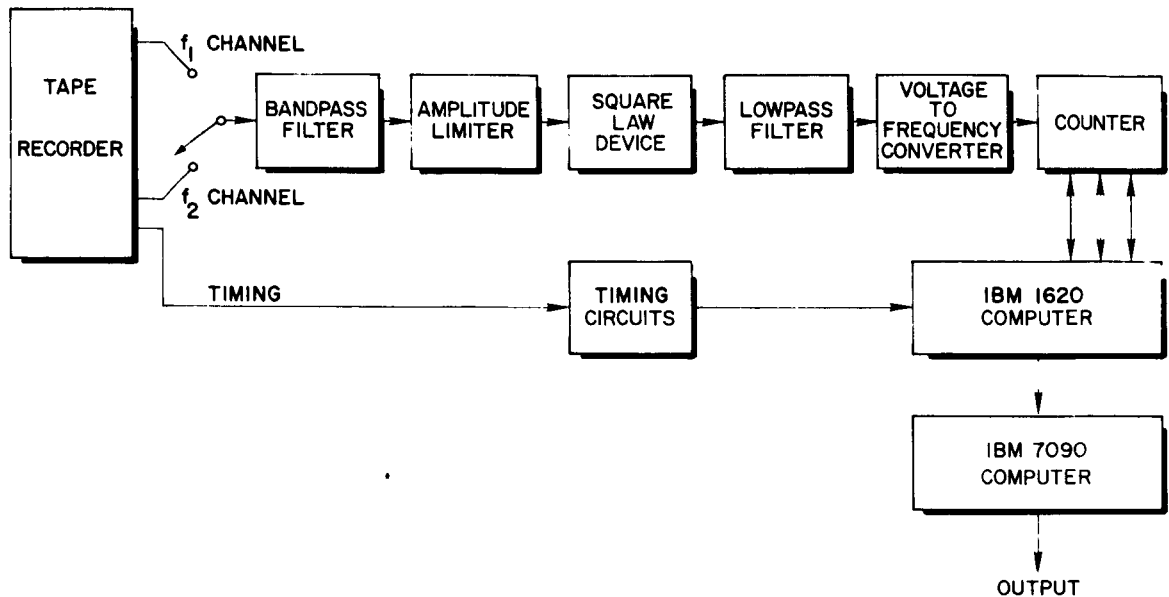


Fig. 2. SIGNAL PROCESSOR BLOCK DIAGRAM.

is proportional to its input voltage level. By counting the pulses for 1 sec, the integral of power for that interval is obtained. Gating, sampling, and resetting of the counter is referenced to the 1 sec clock pulses recorded on the magnetic tape during reception. The numbers obtained are automatically punched on cards. Each of the two channels of data is reduced with this scheme. The cards are fed into an IBM 7090 computer where the data are normalized to account for different gains in equipment at the two frequencies. Subtraction of the two sets of data points for corresponding samples in time is performed. This difference is then digitally correlated against the original transmitted sequence.

A great simplification of the entire system appears in

Fig. 3. That this accurately represents the physical system will be shown later. A short discussion of operation with reference to Fig. 3 will now be given. The transmitter transmits a sine wave at either frequency f_1 or f_2 . The coding is according to the maximum-length sequence signal $s(t)$. In the receiver, the outputs of the square-law detectors give the powers at the two frequencies and their difference gives a replica of the original transmit sequence (plus noise). Crosscorrelation of this difference with the transmit sequence is the optimum detector for small time spread of the returned signal.

The choice of this system was made by considering many aspects of the total problem. The choices of 25 MHz as the operating frequency and use of the log-periodic array instead of the Stanford/SRI 150 ft steerable parabolic-dish antenna were made after an investigation of the effect of frequency and equipment upon signal-to-noise ratio showed these choices to be best [Yoh, 1961].

The choice of a frequency-shifting transmit scheme was made upon consideration of the improvement in signal-to-noise ratio obtained by Barthle [1960] and the successful use of such a system at El Campo. Much of the background noise is nonstationary and contributes power at both frequencies. With a two-frequency system, this component tends to cancel out due to the subtraction of the powers at the two frequencies. This gives a system which is considerably more sensitive than if only a single frequency were used.

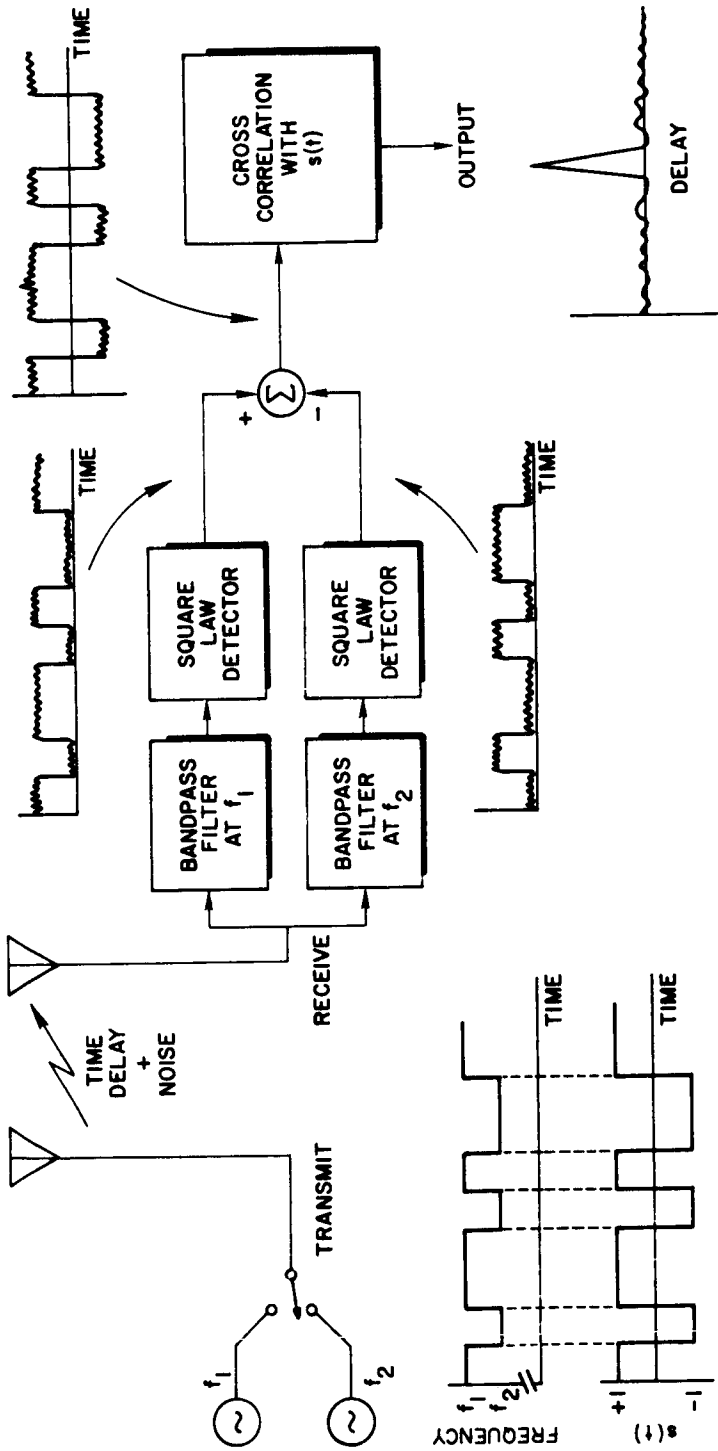


Fig. 3. SIMPLIFIED SYSTEM.

Since the sun was in the fan beam of the antenna for 2 hours each day, it was possible to make two runs per day with the sun in the highest gain portion of the beam. Transmission was for approximately the calculated round-trip time each day (about 1000 sec), with a reception period of the same length.

The noise is principally galactic sky noise plus interference. Solar noise at this frequency is calculated to be only a few percent of the galactic noise, and the sun is not "visible" when it passes through the antenna beam unless it is particularly noisy. Receiver noise is negligible at this frequency. The summer months were chosen for the experiments because then the antenna gain is highest at the high summer elevation angle of the sun. In addition, the background noise level is minimum for that area of the sky in which the sun is located during transit. The minimum effective antenna temperature, corrected for line losses, occurs in August and was typically measured to be 24,000°K.

CHAPTER IV
SYSTEM ANALYSIS

The solar radar system described previously will be analyzed in this chapter. The effects of time spread, doppler spreading and shifting, fluctuations in cross section, Faraday rotation, and a gaussian noise background will be discussed.

The radar cross section of a target is defined as that area normal to the signal path which would produce the actual received power level if the power it intercepted from the transmitter were reradiated isotropically. Accordingly, the standard radar equation is

$$P_r = \frac{P_t G_t}{4\pi R^2} \frac{\sigma}{4\pi R^2} A \frac{1}{2} \quad (2)$$

where P_r = received power
 P_t = transmitted power
 G_t = transmitting antenna gain
 σ = target radar cross section
 A = receiving antenna effective area
 R = target range

The factor of one-half accounts for the fact that a linearly polarized antenna can intercept only half of the energy of a signal whose polarization goes through several rotations during reception. In James [1966] experiments at 38 MHz are

reported which showed that the received signal did indeed go through a sufficient number of polarization cycles such that the signal energies in two quadrature linear polarizations were approximately the same. Whether this was principally due to changes in coronal or ionospheric Faraday rotation is not known.

At 25 MHz the number of rotations in 1000 sec due only to changes in the ionosphere is probably sufficient to make use of this factor reasonable for an individual run, while for the sum of many runs there is no doubt as to its validity. If polarization changes caused by either the corona or the ionosphere cause fading which is fast compared to the length of the signal, then their effect may be included quite accurately by the factor of one-half. The quantitative effect of Faraday-rotation signal modulation will be considered later in detail.

If time spread of the returned signal becomes comparable to the basic pulse length, then the equation must be corrected for the resultant loss of power.

The two-dimensional distribution in time and frequency for the energy of a returned radar signal of short duration is known as the scattering function of a radar target [Green, 1962]. Two one-dimensional functions are satisfactory to describe the present radar system. These are the echo power spectrum $G(f)$ and the power impulse response $h(t)$. The first is the power spectrum of the returned signal if a

continuous sinusoid were the transmitted signal. Figure 4 shows a possible echo power spectrum. The second is the power received as a function of relative delay if a short radio frequency pulse were transmitted. Figure 5 shows a possible $h(t)$. The power impulse response represents a linear filter in terms of power. Thus, returned signal power

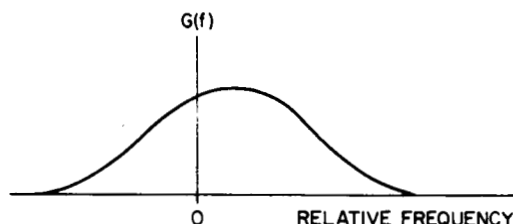


Fig. 4. A POSSIBLE ECHO SPECTRUM.

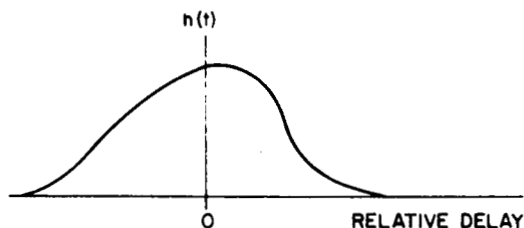


Fig. 5. A POSSIBLE POWER IMPULSE RESPONSE.

is simply a convolution of the power in the transmitted signal with the $h(t)$ for the target. Generally, both of these functions vary with time. Also it must be noted that since a general soft target could produce frequency spreading and time spreading quite independently of each other, the reduction of the scattering function to two one-dimensional

distributions is equivalent to studying a target with a scattering function which is directly factorable into the product of $G(f)$ and $h(t)$. When knowledge of the scattering function can only be crudely estimated, this technique is entirely reasonable.

The coding sequence $s(t)$ is either plus or minus one for 4 sec at a time according to the shift register output. Transmission at frequency f_1 occurs for +1 and f_2 for -1. The normalized analog autocorrelation of $s(t)$ (as derived from the periodic output of the shift register) is

$$\rho(\tau) = \frac{1}{1000} \int_0^{1000} s(t) s(t - \tau) dt \quad (3)$$

The digital form of the signal sequence is defined by

$$s_k = s(t) \quad t \in (k-1, k) \quad (4)$$

The normalized digital autocorrelation of the signal is

$$\rho_j = \frac{1}{1000} \sum_{k=1}^{1000} s_k s_{k-j} \quad (5)$$

This is shown in Fig. 6 for j between ± 100 sec. Each "plateau" represents a point of the digital autocorrelation which is a sampling of the analog autocorrelation function which in turn is actually continuous. This format for correlation plotting will be used henceforth. There are sidelobes

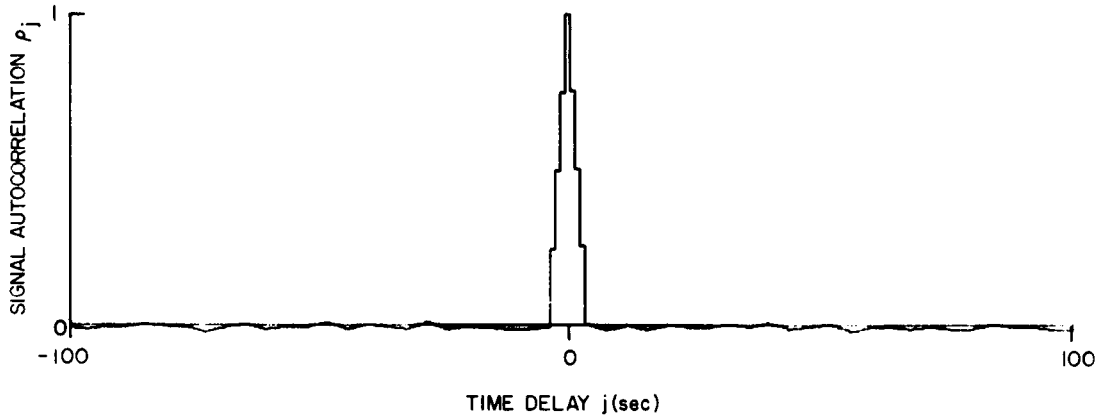


Fig. 6. SIGNAL AUTOCORRELATION.

with about half the amplitude of the central peak at ± 508 and ± 524 sec due to repetition of the sequence nearly twice. The signal arrival time ambiguity is only a few seconds so confusion cannot result.

The transmitted signal, given as voltage on an equivalent 1Ω transmission line, is

$$\begin{aligned}
 T(t) = & \sqrt{2P} s_1(t) \cos (2\pi f_1 t + \phi_1) \\
 & + \sqrt{2P} s_2(t) \cos (2\pi f_2 t + \phi_2)
 \end{aligned}
 \tag{6}$$

where P is the average transmitter power, f_1 and f_2 are the transmitting frequencies, ϕ_1 and ϕ_2 are random phase

angles, while $s_1(t)$ and $s_2(t)$ are the channel signal codings given by

$$s_1(t) = \frac{1}{2} [1 + s(t)]$$

$$s_2(t) = \frac{1}{2} [1 - s(t)]$$
(7)

The receiver model is shown in Fig. 7. For simplicity, the analog signals in the processor are considered to be at the actual received frequencies, instead of in the audio

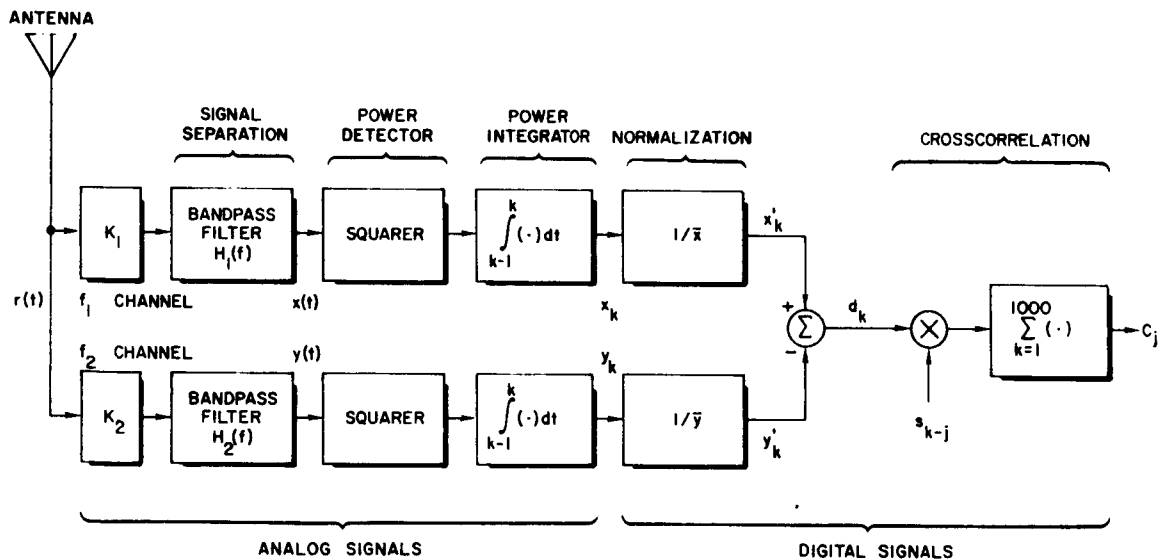


Fig. 7. RECEIVER MODEL.

range as was the actual case, since a translation in frequency does not change the essential character of the signals. K_1 and K_2 represent the (unknown) gains of the two

channels. Normalization of the digital data points in each channel is done by dividing by the mean of each channel. This resolves the values of K_1 and K_2 and accurately balances the effective channel gains. The time index k is an integral number of seconds from some convenient reference. Bandpass filters $H_1(f)$ and $H_2(f)$ have the same shape $H(f)$ relative to the transmitted frequency each is to receive. They incorporate all the frequency characteristics of the system.

Let us assume temporarily that there is no time spread or fading of the signal. Let the noise be additive, stationary, gaussian, zero mean, and with a flat two-sided power spectrum, $N(f)$, of $N_0/2$ watts/Hz over all frequencies of interest. Thus the noise, since it is gaussian, is independent in the two channels. In actuality, the noise is not gaussian as is apparent from the high correlation experienced between the values of x_k and y_k . However, the experimental statistics of the difference d_k between the channels are nearly what is expected for the assumption of gaussian noise at the input. Hence much of the nongaussian noise does cancel out and the initial assumption of gaussian noise is reasonable. The returned signal is modeled as a keyed, narrowband, random signal near each of the transmitted frequencies. The keying of these "random carrier waves" is to correspond to the original transmitter encoding since we are temporarily

neglecting time spread. More precisely, the received signal is assumed to be of the form

$$r(t) = \sqrt{R} s_1(t) g_1(t) + \sqrt{R} s_2(t) g_2(t) + n(t) \quad (8)$$

where s_1 and s_2 are the channel codings (± 1), n is the background noise, and R is the total power in the returned signal. The time functions g_1 and g_2 are assumed to be independent, stationary, zero-mean, gaussian, narrowband random processes with unity average power, which represent the doppler effects produced by the target. When $G_1(f)$ is defined as the power spectrum of $g_1(t)$, then

$$E[g_1^2(t)] = 1 = \int_{-\infty}^{\infty} G_1(f) df \quad (9)$$

where $E[\cdot]$ denotes statistical expectation. $G_1(f)$ and $G_2(f)$ are defined to have the same shape relative to their respective original transmitted frequencies since the transmitted frequencies are closely spaced and the doppler spreading at each frequency will be nearly identical. A possible configuration is shown in Fig. 8. The pairs of frequency functions, G_1 and G_2 , G_1 and H_2 , G_2 and H_1 , H_1 and H_2 , are all assumed to be disjoint. This corresponds to assuming that no energy from one channel overlaps into the other channel. Because the $G_1(f)$ have the same relative shape, the equivalent function $G(f)$ will later be used for all spectral considerations. $G(f)$ is defined as the (bandpass) power

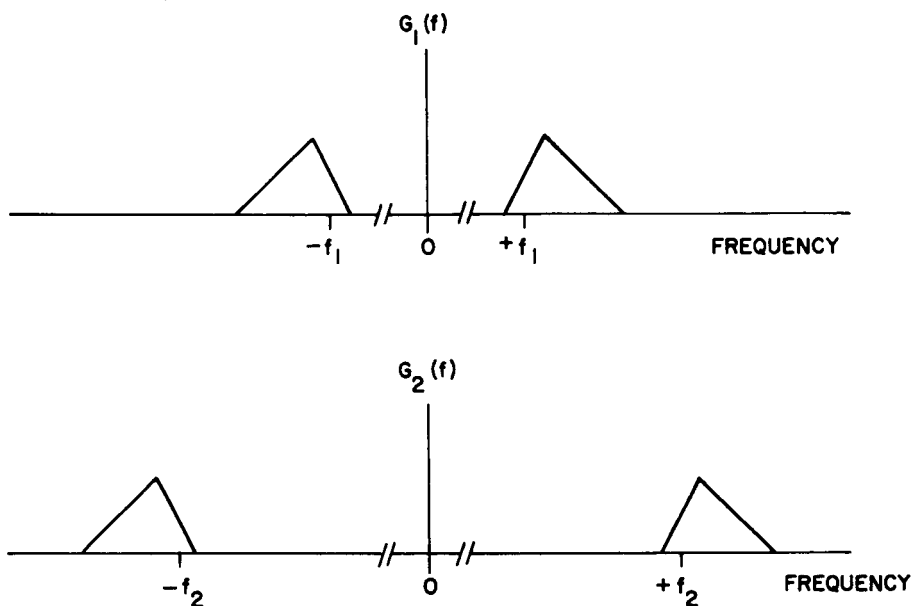


Fig. 8. A POSSIBLE SET OF POWER SPECTRA FOR THE RANDOM CARRIERS.

spectrum of the random carriers, when normalized in frequency to the same single frequency. A similar argument justifies representing $H_1(f)$ and $H_2(f)$ of Fig. 7 by an equivalent $H(f)$, which is still a bandpass function. Let us further define the (single channel) noise bandwidth W of the receiving system as

$$W = \frac{\int_0^{\infty} |H(f)|^2 df}{|H(f_0)|^2} \quad (10)$$

where f_0 is some frequency within the passband of $H(f)$. It is convenient to consider f_0 to correspond to the maximum value of $|H(f)|$. Without loss of generality we may then consider $|H(f_0)|$ normalized to unity. Thus

$$1 = |H(f_0)| \geq |H(f)| \quad (11)$$

and

$$W = \int_0^{\infty} |H(f)|^2 df \quad (12)$$

In the appendix, the system analysis is carried through with the above assumptions and the additional assumption that the average input signal-to-noise power ratio is significantly less than unity. The signal component of the correlation output C_j is shown to be

$$E[C_j] = 10^3 \frac{\beta R}{N_0 W} \rho_{j-(T_R-T_0)} \quad (A-26)$$

where β is that fraction of the total received power R that is passed through the filtering characteristics of the system and is defined by [cf. (A-13)]

$$1 \geq \beta = \int_{-\infty}^{\infty} G(f) |H(f)|^2 df \quad (13)$$

$\rho_{j-(T_R-T_0)}$ is the normalized signal autocorrelation shifted by $T_R - T_0$, where T_R is the signal round-trip time and T_0 is the processor's time origin. Since $T_R - T_0$ is generally not an integer, the subscript $j-(T_R-T_0)$ implies sampling of the continuous signal autocorrelation function at a nonintegral value of shift.

The noise component of C_j is shown to be

$$\text{Var } [C_j] = \frac{10^3}{W^2} \int_{-\infty}^{\infty} |H(f)|^4 df \quad (\text{A-44})$$

This noise is dependent only upon the shape of the effective system passband.

Let us define an effective input signal-to-noise ratio as the ratio of total signal power entering the system to total noise power entering the system. Since R is the total signal power coming from the antenna and β is that fraction entering the system, clearly βR is the input signal power. W has been defined as the effective noise bandwidth; so, since there are two channels intercepting $N_0/2$ watts/Hz for positive and negative frequencies, the total noise power is $2N_0W$ and the effective input SNR is

$$\text{SNR}_{in} = \frac{\beta R}{2N_0W} \quad (14)$$

For maximization of SNR_{in} , it is not possible in general to simply increase the bandwidth to make $\beta \rightarrow 1$, since the denominator will likewise increase. Let us now define and examine the output SNR. The signal output is $E[C_j]$. The power may be defined as the square of the height of the maximum value, i.e., where $\rho = 1$ due to an argument of zero. The noise power may be defined as the variance of C_j . Therefore the output SNR is

$$\begin{aligned}
\text{SNR}_o &= \frac{10^6 (\beta^2 R^2 / N_o^2 W^2)}{\frac{10^3}{W^2} \int_{-\infty}^{\infty} |H(f)|^4 df} \\
&= \frac{10^3 R^2 \beta^2}{N_o^2 \int_{-\infty}^{\infty} |H(f)|^4 df} \tag{15}
\end{aligned}$$

The optimum $H(f)$ to maximize SNR_o may now be found.

$$\text{SNR}_o = \frac{10^3 R^2}{N_o^2} \frac{\left[\int_{-\infty}^{\infty} G(f) |H(f)|^2 df \right]^2}{\int_{-\infty}^{\infty} |H(f)|^4 df} \tag{16}$$

If we multiply the numerator and denominator by $\int_{-\infty}^{\infty} G^2(f) df$ and use the Cauchy-Schwarz inequality wherein for any real α and γ

$$\frac{\left[\int_{-\infty}^{\infty} \alpha(\xi) \gamma(\xi) d\xi \right]^2}{\int_{-\infty}^{\infty} \alpha^2(\xi) d\xi \int_{-\infty}^{\infty} \gamma^2(\xi) d\xi} \leq 1 \tag{17}$$

(with equality if and only if $\alpha = K\gamma$, with K equal to any constant), then the following inequality holds

$$\text{SNR}_0 = \frac{10^3 R^2}{N_0^2} \int_{-\infty}^{\infty} G^2(f) df \left\{ \frac{\left[\int_{-\infty}^{\infty} G(f) |H(f)|^2 df \right]^2}{\int_{-\infty}^{\infty} G^2(f) df \int_{-\infty}^{\infty} |H(f)|^4 df} \right\}$$

$$\leq \frac{10^3 R^2}{N_0^2} \int_{-\infty}^{\infty} G^2(f) df \quad (18)$$

where $G \rightarrow \alpha$, $|H|^2 \rightarrow \gamma$, and the quantity in braces is less than or equal to one. The maximum value of SNR_0 is obtained if and only if $|H(f)|^2$ is chosen to be proportional to $G(f)$. Then

$$\text{SNR}_{0_{\max}} = \frac{10^3 R^2}{N_0^2} \int_{-\infty}^{\infty} G^2(f) df \quad (19)$$

Since $\int_{-\infty}^{\infty} G(f) df$ is unity, it is seen that the maximum SNR_0 is strongly dependent upon how the area underneath the $G(f)$ curve is distributed. Clearly if $G(f)$ is concentrated in a very narrow band, much less noise has to be admitted in order to obtain most of the signal energy than if $G(f)$ were widely spread. Thus a higher $\text{SNR}_{0_{\max}}$ would result.

A. Time Spreading Effects

The effect of time spreading upon detection of the returned signal may now be examined. Let the power of a transmitted signal be $s(t)$ in time. Then, as mentioned earlier, we may find the power vs time of the returned

signal by a convolution with the power impulse response of the target. Hence reflected power as a function of time is

$$P(t) = \int_{-\infty}^{\infty} h(\xi) s(t-\xi) d\xi \quad (20)$$

This is the situation existing with the present system, if $s(t)$ is the coding sequence and $P(t)$ is understood to be the signal (and allowed to be negative) just after channel subtraction (see Fig. 3).

Let us consider the crosscorrelation operation in terms of continuous signals. There is complete equivalence between a continuous and a digital formulation of this operation, the latter simply being a sampling of the former. The operation (ignoring the constant factors) then is

$$\begin{aligned} C(\tau) &= \int_0^T P(t) s(t-\tau) dt \\ &= \int_0^T \int_{-\infty}^{\infty} h(\xi) s(t-\xi) s(t-\tau) dt d\xi \\ &= \int_{-\infty}^{\infty} h(\xi) \int_0^T s(t-\xi) s(t-\tau) dt d\xi \quad (21) \end{aligned}$$

By a change of variable $\gamma = t-\xi$,

$$C(\tau) = \int_{-\infty}^{\infty} h(\xi) \int_{-\xi}^{T-\xi} s(\gamma) s(\gamma+\xi-\tau) d\gamma d\xi \quad (22)$$

The nonzero extent (i.e., time spread) of $h(\xi)$ is, at most, several seconds. Therefore, for $T = 1000$, a very small

error is introduced if the limits of the inner integral are changed to $[0, T]$. Thus, for $T = 1000$,

$$C(\tau) = \int_{-\infty}^{\infty} h(\xi) \int_0^{1000} s(\gamma) s[\gamma - (\tau - \xi)] d\gamma d\xi \quad (23)$$

The inner integral is recognized as the signal auto-correlation, $10^3 \rho(\tau - \xi)$. Thus

$$C(\tau) = 10^3 \int_{-\infty}^{\infty} h(\xi) \rho(\tau - \xi) d\xi \quad (24)$$

and we observe a convolution of the transmit sequence auto-correlation function with the power impulse response of the target.

Returning to the digital crosscorrelation scheme, we observe that no problems have been created, since the digital technique simply evaluates $C(\tau)$ for integral values of τ . Time spreading due to the target is thus observable as the departure from the ideal shape of the crosscorrelation curve.

If the power impulse response of the target were known exactly, then the optimum correlation scheme (for a given transmitted signal) would crosscorrelate the returned signal power with a replica of the transmitted signal coding which has been convolved with $h(t)$. Since the results of correlation detection and "matched filtering" are identical, we see that this deliberate distortion of the "stored" signal will maximize the output SNR via the matched filter concept [Davenport and Root, 1958]. It should be noted that this is

a true optimization only if the noise entering the correlation scheme is essentially white. If it were not, a "prewhitening" or "bleaching" filter would be necessary after the squaring operation. For a narrowband gaussian noise process with the power spectral density shown in Fig. 9a, the power spectrum of its square (after filtering out the double frequency term) can be shown to be as in Fig. 9b [Davenport and Root]. The

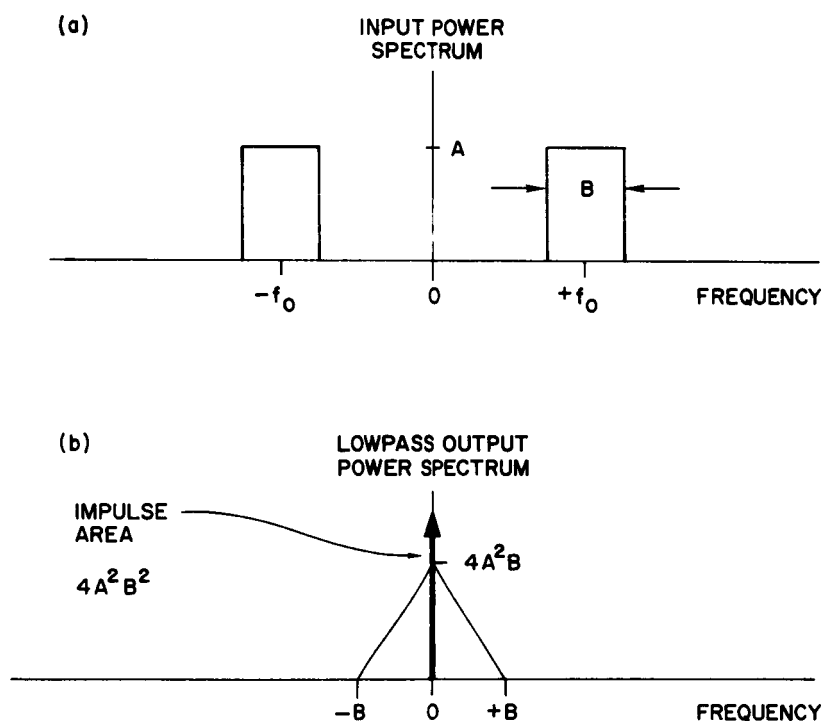


Fig. 9. INPUT AND OUTPUT POWER SPECTRA FOR SQUARE-LAW DETECTION.

output spectrum obviously is not white. However, the impulse is removed when the two channels are subtracted. In addition, since the signal bandwidth is of the order of the inverse of the pulse length, the effective bandwidth of the equivalent

matched filter is several orders of magnitude smaller than the bandwidth B of Fig. 9b. Thus the correlation operation sees noise which is essentially white with a power spectral density approximately equal to $4A^2B$, and no prewhitening is necessary.

If both the echo power spectrum and the power impulse response are known (and their product is the scattering function), then the optimum system for maximum output SNR (for a fixed signal) consists first of an input filter $|H(f)|$ equal to the square root of the echo spectrum and a power detector. Correlation with the transmitted signal is then performed after it has first been convolved with the power impulse response.

The problem of choosing a pulse length for maximizing detectability is easily considered but not readily resolved. Observe from Eq. (24) that to maximize $C(0)$, since $h(t)$ is fixed, we simply desire $\rho(-\xi)$ to be as large as possible over the range of nonzero $h(\xi)$. Since ρ is limited to unity, this corresponds to making $\rho \approx 1$ over the range of nonzero h . This cannot be done exactly, and can be approached only to the extent that time resolution is sacrificed. However, for pulse lengths much longer than the time spread, maximum detectability is essentially obtained. The desire for resolution of the time spread calls for pulse lengths shorter than the spread, which reduces the output SNR due to the overlapping of pulse intervals.

B. Amplitude Fluctuations of the Received Signal

As mentioned previously, amplitude fading of the returned signal is certain to exist, if only from Faraday rotation in the earth's atmosphere which causes polarization misalignment when an antenna of only one linear polarization is used for reception. If a dual-polarization receiving system were employed and the two polarization powers summed, then the fading effects of Faraday rotation (both earth and/or solar) could be eliminated.

The effect of Faraday rotation (for a single linear polarization) is a time-varying (power) gain with a range of $[0, 1]$ and an average value of one-half. The daily variation of measured cross section at El Campo indicates that changes of cross section within hours are probable. Variations within minutes and seconds should be considered a possibility until results show otherwise.

If it is assumed that both channels are affected equally by fading, then at the point after channel subtraction the returned signal (normalized) may be considered to be $f(t)\alpha(t)s(t)$, where $f(t)$ is the Faraday (earth and/or solar) fading power gain factor (limited to $[0,1]$), $\alpha(t)$ is the instantaneous cross section of the corona, and $s(t)$ is the transmit encoding. Observe that $f(t) \geq 0$ and $\alpha(t) \geq 0$, while $s(t)$ can be positive and negative. Time spread is assumed negligible. If the changes in reflected power level are slow enough so that a receiver's bandwidth may follow

them, we are justified in defining an instantaneous cross section. Any measurement of cross section is a time average of $\alpha(t)$ over the signal interval. If $\alpha(t)$ can vary significantly during a day, then the measured value of cross section may bear little resemblance to that value which might be considered the average cross section for that day. The ideal measurement would be to obtain $\alpha(t)$ exactly, but if this is not possible, an understanding of what actually is being done is necessary. The quantity $\alpha(t)$ should be modeled as a nonstationary random process since stationarity does not seem reasonable here due to the correlation experienced between cross section and solar activity. The concept of an average value of $\alpha(t)$ thus becomes somewhat ambiguous because a "time average" is now a function of time. To circumvent this difficulty, quasi-stationarity of $\alpha(t)$ will be assumed. If only one run were made per day, it would be desired that the cross-section measurement be representative of $\alpha(t)$ for the entire day. Thus we could consider the quasi-stationary mean $E[\alpha(t)] = \bar{\alpha}$ to be the average of the true nonstationary process over one day. $\alpha(t)$ will fluctuate about this mean and will [in conjunction with $f(t)$] produce errors in estimates of $\bar{\alpha}$ when a reflected signal is analyzed.

The crosscorrelation processing is (ignoring a constant factor)

$$C(\tau) = \int_0^T [f(t) \alpha(t) s(t)] s(t-\tau) dt \quad (25)$$

The signal component of $C(\tau)$ is

$$E[C(\tau)] = \int_0^T E[f(t)]E[\alpha(t)] s(t) s(t-\tau) dt = \bar{f}\bar{\alpha}T\rho(\tau) \quad (26)$$

Thus the output is proportional to the average cross section. Since the average of f is one-half, this produces the factor of one-half in the radar equation (2) as previously discussed.

Of interest is the variance of $C(\tau)$ produced by f and α . The function f is assumed to be a stationary random process so that both f and α have autocorrelation functions given by

$$R_f(\tau) = E[f(t) f(t+\tau)] \quad (27)$$

$$R_\alpha(\tau) = E[\alpha(t) \alpha(t+\tau)] \quad (28)$$

It is convenient to define

$$z(t) = f(t) \alpha(t) \quad (29)$$

Hence

$$R_z(\tau) = R_f(\tau) R_\alpha(\tau) \quad (30)$$

The variance of $C(\tau)$ is given by

$$\begin{aligned}
\text{Var}[C(\tau)] &= E \left\{ \left[\int_0^T z(t) s(t) s(t-\tau) dt \right]^2 \right\} - E^2[C(\tau)] \\
&= \int_0^T \int_0^T E[z(t) z(\xi)] s(t) s(t-\tau) s(\xi) s(\xi-\tau) dt d\xi \\
&\quad - E^2[C(\tau)] \tag{31}
\end{aligned}$$

Since interest centers on the error in estimating the cross section, evaluation of $\text{Var}[C(0)]$ is desired (assuming that the signal peak is at zero shift). Thus

$$\text{Var}[C(0)] = \int_0^T \int_0^T E[z(t) z(\xi)] s^2(t) s^2(\xi) dt d\xi - E^2[C(0)] \tag{32}$$

Since $s(t)$ is ± 1 and the expectation gives the autocorrelation of z ,

$$\text{Var}[C(0)] = \int_0^T \int_0^T R_z(t-\xi) dt d\xi - E^2[C(0)] \tag{33}$$

A change of variable, $\phi = t-\xi$, gives

$$\text{Var}[C(0)] = \int_0^T \int_{-\xi}^{T-\xi} R_z(\phi) d\phi d\xi - E^2[C(0)] \tag{34}$$

The cases of slow and fast fading may now be examined. We may speak of a "fading time" t_0 as that time separation between values of $z(t)$ such that they are nearly independent. It is obtained (qualitatively in this discussion) as that time where $R_z(\tau)$ approaches $R_z(\infty) = \bar{z}^2$. See Fig. 10 for an example.

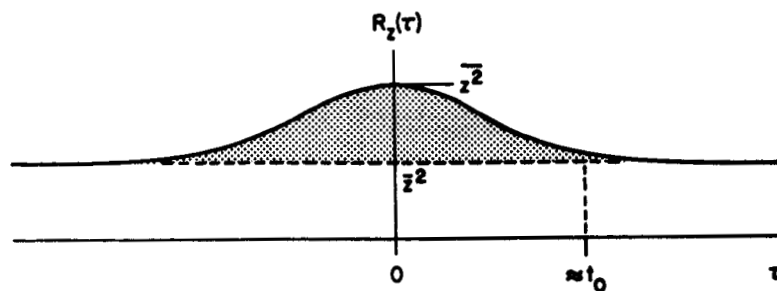


Fig. 10. A POSSIBLE FADING AUTOCORRELATION FUNCTION.

Slow fading is the case where $t_0 \gg T$ [$z(t)$ is correlated over long periods compared to T]. Thus $R_z(\phi) \approx R_z(0)$ in the inner integral of Eq. (34); and since $R_z(0) = \bar{z}^2$, we obtain

$$\begin{aligned}
 \text{Var}[C(0)] &= T^2 \overline{z^2} - E^2[C(0)] \\
 &= T^2 \overline{z^2} - [\bar{z} \overline{Tp(0)}]^2 \\
 &= T^2 [\overline{z^2} - \bar{z}^2] \\
 &= T^2 \text{Var}[z]
 \end{aligned} \tag{35}$$

For the case of fast fading, we first define

$$\hat{R}_z(\tau) = R_z(\tau) - \bar{z}^2 \tag{36}$$

Then Eq. (34) becomes

$$\text{Var}[C(0)] = \int_0^T \int_{-\xi}^{T-\xi} \hat{R}_z(\phi) d\phi d\xi + \int_0^T \int_{-\xi}^{T-\xi} \bar{z}^2 d\phi d\xi - E^2[C(0)]$$

$$= \int_0^T \int_{-\xi}^{T-\xi} \hat{R}_z(\phi) d\phi d\xi \quad (37)$$

For fast fading, $t_0 \ll T$, therefore, the inner integral limits can be changed to $\pm\infty$ with negligible error.

$$\begin{aligned} \text{Var}[C(0)] &= \int_0^T \int_{-\infty}^{\infty} \hat{R}_z(\phi) d\phi d\xi \\ &= T \int_{-\infty}^{\infty} \hat{R}_z(\phi) d\phi \end{aligned} \quad (38)$$

The latter integral is the shaded area in Fig. 10 and is proportional to $t_0(\overline{z^2} - \bar{z}^2)$, where the constant of proportionality depends only upon the generic form of $R_z(\tau)$. If $R_z(\tau)$ is assumed to have the simple triangular shape of Fig. 11, the constant is unity. Therefore

$$\text{Var}[C(0)] = T t_0 \text{Var}[z] \quad (39)$$

For an $R_z(\tau)$, where t_0 cannot be explicitly determined, it is possible to always make the proportionality constant

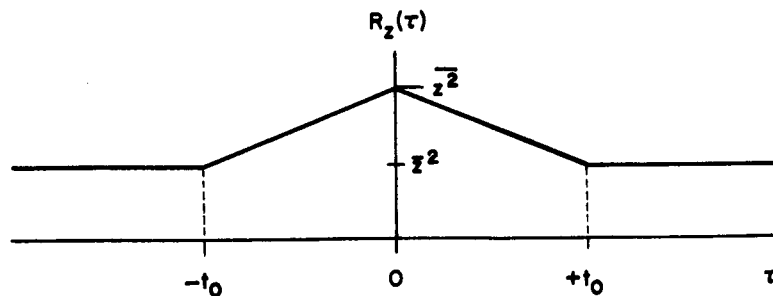


Fig. 11. A TRIANGULAR FORM OF THE FADING AUTOCORRELATION FUNCTION.

unity and to define t_0 such that this is true. If this is done for an $R_z(\tau)$ consisting of a gaussian curve on top of \bar{z}^2 , it is found that t_0 corresponds to the 2.5 standard deviations point on the gaussian curve and at that point is reduced to 4.3 percent of its peak value. This interpretation should be considered as a definition of t_0 for the following results. In summary:

$$\text{Var}[C(0)] = \begin{cases} T^2 \text{Var}[z] & \text{slow } (t_0 \gg T) \\ Tt_0 \text{Var}[z] & \text{fast } (t_0 \ll T) \end{cases} \quad (40)$$

We may define the normalized standard deviation of the error by

$$\sigma_E = \frac{\sqrt{\text{Var}[C(0)]}}{E[C(0)]} = \begin{cases} \frac{\sqrt{\text{Var}[z]}}{E[z]} & \text{slow} \\ \sqrt{\frac{t_0}{T}} \frac{\sqrt{\text{Var}[z]}}{E[z]} & \text{fast} \end{cases} \quad (41)$$

If we define a normalized standard deviation of the fading function as

$$\sigma_z = \frac{\sqrt{\text{Var}[z]}}{E[z]} \quad (42)$$

we then have

$$\frac{\sigma_E}{\sigma_z} = \begin{cases} 1 & \text{slow } (t_0 \gg T) \\ \sqrt{\frac{t_0}{T}} & \text{fast } (t_0 \ll T) \end{cases} \quad (43)$$

Thus we have the fractional error of the cross section related to the fractional variation of the fading function in terms of the fading time and the length of the signal. This result has general application to any system.

For comparison purposes, the exact solution of σ_E/σ_Z using the autocorrelation function of Fig. 11 has been carried through beginning with Eq. (34). The result, with all terms defined as above, is

$$\frac{\sigma_E}{\sigma_Z} = \begin{cases} \sqrt{1 - \frac{T}{3t_0}} & (T \leq t_0) \\ \sqrt{\frac{t_0}{T}} \sqrt{1 - \frac{t_0}{3T}} & (T \geq t_0) \end{cases} \quad (44)$$

In Fig. 12, σ_E/σ_Z from Eq. (43) for various values of T and t_0 is plotted for the slow and fast fading cases (solid lines). The exact solution for the triangular autocorrelation function is plotted as dashed lines and is probably representative of the exact results obtainable from the class of autocorrelation functions which are well behaved in the sense of not having any sidelobes comparable to $R_Z(0)$.

For an example using Fig. 12, let $t_0 = 100$ sec with a 1000 sec signal. The value of σ_E/σ_Z is then approximately 0.3. If the standard deviation of the fading factor were 50 percent of its average value, we could expect the error in the measurement of the cross section to have a standard

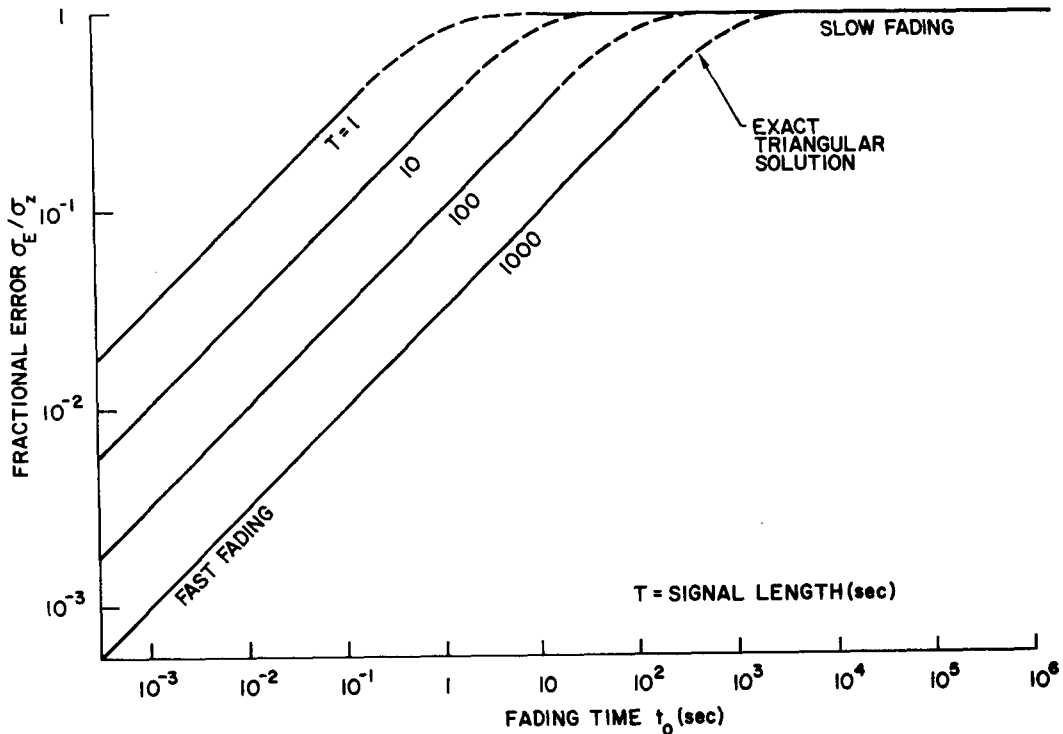


Fig. 12. FRACTIONAL MEASUREMENT ERROR AS A FUNCTION OF FADING TIME AND SIGNAL LENGTH.

deviation of 15 percent relative to the true cross-section value.

It should be noted that since $R_z(\tau)$ is the product of $R_f(\tau)$ and $R_\alpha(\tau)$, the fading time of $R_z(\tau)$ is essentially determined by the minimum value of the fading times for f and α individually, with this approximation becoming exact as the ratio of individual fading times becomes large. Thus we see that if both $f(t)$ and $\alpha(t)$ change very slowly, measurement errors will be large, while if either changes very fast, the error will be small. If a dual polarization

system is used, $f(t) = 1$ and $R_z(\tau) = R_\alpha(\tau)$.

While $R_\alpha(\tau)$ is essentially an unknown function of the corona, $R_f(\tau)$ can be established quite well from the assumptions made above. We have assumed that $f(t)$ is a stationary random process restricted to the range $[0, 1]$. It arises as the square of the sine of a phase angle which we shall assume to be uniformly distributed over $[0, 2\pi]$. Thus

$$f(t) = \sin^2 \theta(t) \quad (45)$$

where the probability density of θ is

$$p_\theta(\theta) = \frac{1}{2\pi} \quad \theta \in [0, 2\pi] \quad (46)$$

Hence

$$E[f(t)] = \frac{1}{2} \quad (47)$$

Using Parzen [1960], the probability density of f may be readily found to be

$$p_f(f) = \frac{1}{\pi\sqrt{f(1-f)}} \quad f \in [0, 1] \quad (48)$$

The mean square value of f is

$$E[f^2] = \int_0^1 f^2 p_f(f) df = \int_0^1 \frac{f^2}{\pi\sqrt{f(1-f)}} df = \frac{3}{8} \quad (49)$$

Thus

$$\text{Var}[f] = E[f^2] - E^2[f] = \frac{1}{8} \quad (50)$$

If $\alpha(t)$ is fixed and equal to unity, then from Eq. (42)

$$\sigma_z = \frac{\sqrt{\text{Var}[f]}}{E[f]} = \sqrt{\frac{1}{2}} \quad (51)$$

Thus, in addition to causing a loss of half of the power for a linear polarized antenna, Faraday rotation can also cause substantial measurement errors. Consider a fading time of 300 sec and a signal of 1000 sec duration. With σ_z as above, then σ_E , the standard deviation of the error, is 40 percent of the actual cross-section value.

When the total columnar electron content of the signal path is changing linearly with time, the polarization angle will also change linearly. If this holds true over a signal interval,

$$f(t) = \cos^2 (\omega_0 t + \theta) \quad (52)$$

where θ is a random phase angle which is uniformly distributed on $[0, 2\pi]$. Then it can be directly found that

$$R_f(\tau) = \frac{1}{4} + \frac{1}{8} \cos 2\omega_0 \tau \quad (53)$$

If $\alpha(t)$ is assumed to be unity, we may evaluate Eq. (34) for this form of $f(t)$. The evaluation is straightforward and produces

$$\text{Var}[C(0)] = \frac{\sin^2 \omega_0 T}{8\omega_0^2} \quad (54)$$

For very slow fading, ω_0 approaches zero and

$$\lim_{\omega_0 \rightarrow 0} \text{Var}[C(0)] = \frac{T^2}{8} \quad (55)$$

Since $\text{Var}[z]$ is $1/8$ [Eq. (50)], Eq. (55) thus agrees with Eq. (40) in the slow fading case. For the fast fading case, t_0 may reasonably be defined as the time between an adjacent minimum and maximum of $f(t)$. Hence t_0 becomes $\pi/2\omega_0$. Thus for the squared sinusoid form of $f(t)$, the output variance when compared to the completely random case is smaller (for fast fading) by a factor of

$$\frac{2 \sin^2 \omega_0 T}{\pi \omega_0 T} < 1 \quad (56)$$

The expression for fractional error can be evaluated and is

$$\frac{\sigma_E}{\sigma_z} = \frac{|\sin \omega_0 T|}{\omega_0 T} \quad (57)$$

Since σ_z is known,

$$\sigma_E = \sqrt{\frac{1}{2}} \frac{|\sin \omega_0 T|}{\omega_0 T} \quad (58)$$

The reason for the squared sinusoid form of $f(t)$ giving a smaller error is because its structure forces it to be a better "averager" than a completely random process.

The assumption of quasi-stationarity for $\alpha(t)$ creates

a problem when more than one run is made on a given day, since we are now able to make several estimates of $\alpha(t)$ at slightly different times. If several measurements near the same time give nearly identical results, then the quasi-stationary assumption would appear to be justified and t_0 and/or σ_z must be quite small.

If a large scattering of measured values results from several successive measurements, then from the standard deviation of the measured values and by use of Fig. 12, a relation between t_0 and σ_z may be obtained. If a succession of measured values displayed a somewhat steady progression, this would indicate that the cross section was indeed changing and the quasi-stationary assumption would clearly be in error. It would be apparent, however, that t_0 and/or σ_z were small or this could not be observed.

From the analysis above, the effect of various assumed modes of behavior for ionospheric fading and cross-section fluctuations may be readily evaluated. From the analysis, we see that the measurement of cross section obtained is exactly the time average of $\alpha(t)$ over the signal interval. The error we have evaluated is in terms of how well this measurement represents the average value of the cross section over periods of time much larger than a signal interval.

CHAPTER V

SYSTEM VALIDATION

The claim will be made in Chapter VI that the data taken and analyzed with the Stanford solar radar show that the radar cross section of the sun was below the system's sensitivity to detect, even when many runs were summed. Before this can be accepted as probable, a substantial effort must be made to prove the validity of the system as a properly functioning radar. This will now be done. A description will be given of the techniques used to maintain time synchronization, frequency accuracy, and antenna alignment. The use of several sets of our artificial data and actual data from the El Campo installation to check the system will also be discussed.

The computational scheme for determining the phasing of the antenna elements for a celestial target during transit has been fully verified by over 5 years of extensive lunar radar investigations (see references listed under Stanford Radioscience Laboratory). The phasing calculations used in the solar work have since been independently recalculated and are in agreement with those used during the experiments. Since the elevation of the sun is high during the summer months, ionospheric refraction is quite small, but a correction was made to account for this effect. The correction scheme was the same as applied to the lunar work.

The gain of the antenna was measured by comparing moon

bounce signal strength to that obtained with a reference dipole. The measured gain was 25.3 dB over isotropic. This value compared very well with the theoretical design gain of 25.9 dB [Howard, 1965], which shows that the phasing calculations give the proper beam positioning. A further verification of pointing accuracy was that the measured moon signals consistently gave a lunar radar cross section of 7 percent of the physical cross section.

During a solar run, the transmitter power level was continuously monitored. With the power level used, if the power was for some reason being dissipated elsewhere than the antenna, it would be readily apparent by the smoke and/or fire. This same transmitter at the same frequency and with the same power output was used for the successful lunar work.

The transmitter coding was checked by comparing the strip chart record of the keying with the correct sequence. In addition, since the tape recorder was started before the transmitter stopped, an independent check upon the transmitter operation could be made. Such a check was possible because the receivers, although isolated as much as possible from the transmitter, nevertheless picked up the signal and recorded it on the tape, thus allowing the transmitter frequency shifting to be checked with reference to the timing and reference pulses recorded on the tape. The strip chart also had the timing and reference pulses recorded upon it. The reference pulses were always begun at a preselected time with

reference to the transmit beginning. Thus, by checking the strip chart and the magnetic tape, the absolute time reference could be verified and this was done for every run.

From observing the actual frequency of the tail end of the transmit signal on the tape, it could be determined if the receivers and the transmitter had the proper frequency relationship and that the mixing operations in the receiver were proper. To preserve the proper sense of frequency on the tape, the receiver must equivalently perform a "low-side" mixing operation. Then if a receiver was tuned higher than a transmitted sine wave signal, the frequency of the sine wave on the tape would be lower by the same amount when compared to the tape frequency which corresponds to the receiver's intermediate frequency. (See Table 1.) The tape recorder zero-doppler frequency is the frequency actually found at the beginning of the tapes due to the transmitter. This observation showed that the receivers and the transmitter were properly tuned.

Processing of the data, which was not done in real time, critically depended upon the time reference recorded on the tape during reception. Absolute timing was derived from the first clock pulse after an unambiguous step in the timing channel. Relative timing was then derived from the ensuing pulses at the 1 sec clock rate. Each clock pulse produced a data point (x_k or y_k). Any excess or deficiency of pulses would cause signal distortion and loss of absolute

timing. To combat possible noise in the timing channel, a scheme was used whereby single clock pulses could be accepted at a rate only slightly faster than the nominal 1 Hz rate. If noise pulses were present, they would be ignored unless they occurred just prior to a true pulse. In this case, the noise pulse would trigger the sampling and the true pulse would be ignored. A very small error would exist in two successive data points, but absolute timing would be maintained. Up to several seconds of continuous noise in the timing channel could be tolerated with this scheme, producing only small errors in the sampled points but ensuring accurate timing. Only a very small number of runs actually required this scheme, but it was used to guarantee that timing was properly maintained. In the unlikely event of the loss of one or more clock pulses, the problem would be apparent by large deviations of the data points from the average. All runs with such deviations were checked and in only one case was the loss of a time pulse responsible. For the other runs, no time pulses were missing in the vicinity of the large deviations. High levels were seen in the data channels, however, and thus these large values represented the true data. To substantiate this finding, the runs were reduced again and gave identical results.

Several schemes were used to check the entire system. The data processing program for the IBM 7090 computer had a self-checking routine which constructed an artificial signal

and performed the crosscorrelation. Several artificial signals were constructed on magnetic tape and used for checking the processing. Two noise-free test signals were recorded with the signal specifically located with respect to the standard timing format. These signals provided an accurate assessment of the processor's timing. In addition, three tests were run using the entire receiving system, including the antenna. The shift register was used to switch between two signal generators in order to construct the signal which was then connected to a small antenna on the roof of the station. This antenna was aimed toward the log-periodic array, which was phased as for a normal data run. The amplitude was first adjusted so that the signal and noise power levels in the receivers were equal and then was attenuated by the desired amount. The standard timing format was used, with the processor time origin identical with the beginning of the "transmitted" signal. The resultant crosscorrelation for a test signal which was 23 dB below the noise [as defined by Eq. (14)] is shown in Fig. 13. Interference was severe during the tests and produced large fluctuations in the output. The outputs of the processor for all test runs gave results in close agreement with the input signal levels.

For actual data runs that were relatively free from interference, the variance of the difference between the channels d_k and the correlation output C_j were very close to that calculated for gaussian noise in Chapter IV. The

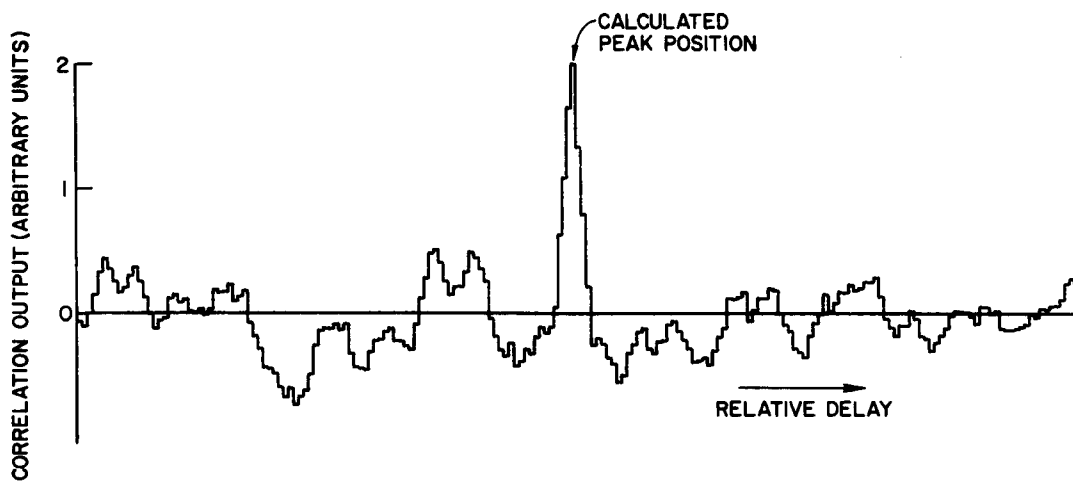


Fig. 13. TEST SIGNAL OUTPUT CORRELATION.

variance of the data points x_k and y_k was generally considerably larger than that which a gaussian noise input would be expected to produce. The correlation coefficient between the set of data points x_k, y_k for each channel was calculated for all runs and the figure obtained was generally above 0.9 with values of 0.96 to 0.99 being quite typical. The high variance of each channel is due to a lack of statistical stationarity in the input noise. However, the non-stationary component apparently cancels out quite well and justifies the approximation of the input noise by a gaussian process. The high correlation between 16 kHz bandwidth channels spaced 50 kHz apart is seen by comparing the plots in Fig. 14a, b. These plots are of x_k and y_k for 1,000

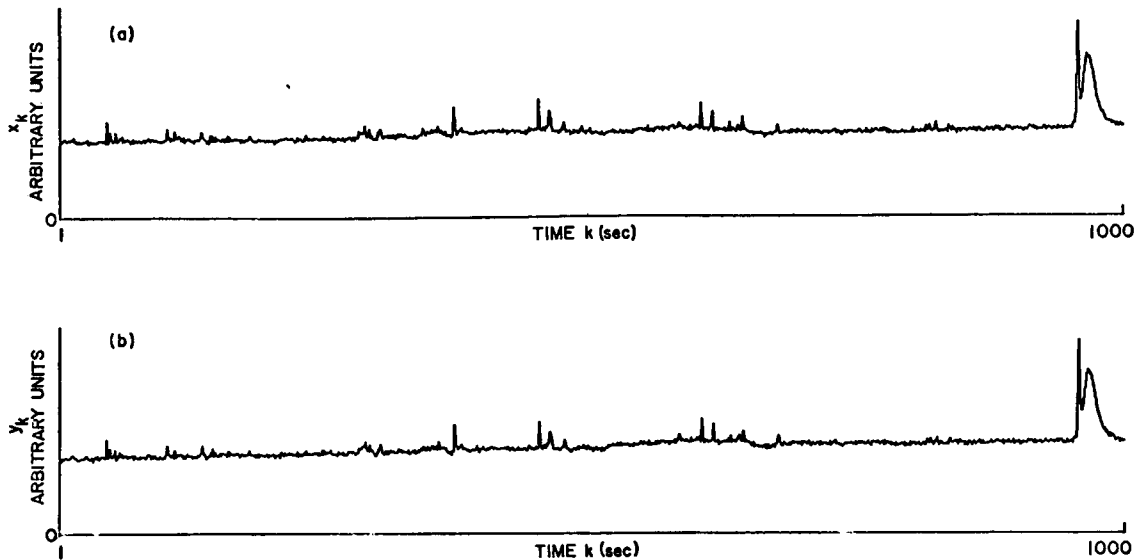


Fig. 14. TYPICAL DATA FROM A RUN IN THE 1965 SERIES (TAPE 589-2).

data points for a typical run from the 1965 series. It is difficult to see differences between the plots. The correlation coefficient for this run was calculated to be 0.990.

The test tapes were reduced at regular intervals during actual data reduction to check upon the processor's performance. In addition to the checks above, a series of plots for every run was produced by an automatic digital plotter which showed the values of x_k , y_k , d_k , and C_j . The means and variances of these variables were computed as well, which then allowed extensive comparison with expected results.

For a final check upon the signal processing, actual solar radar data, which were kindly furnished by the El Campo installation, were reduced with the Stanford signal processor. The transmitted signal used to obtain the data was nearly

identical with the Stanford signal, and the data format was quite similar. Thus, only small changes were necessary in order to reduce the data. The results of two data tapes are plotted in Figs. 15 and 16 together with the results from the same data when reduced at the El Campo facility. The plots were scaled so as to agree at the peak value of the El Campo data when the Stanford points were connected by straight lines. The Stanford reduction was done with a somewhat wider bandwidth, and in the case of tape EC-43, a very noisy portion of the original data was rejected. This accounts for the smaller general noise level in the Stanford reductions and in particular, the elimination of a large noise peak in Fig. 15. The time scale for the Stanford data points, which was derived independently of the El Campo results, utilized only an absolute timing reference provided by a single pulse on the tape. Relative timing was obtained from a 1 kHz recorded clock which was subdivided to provide 1 sec pulses. The calculations of returned signal levels agreed fairly well with the El Campo results and corresponded to a radar cross section on the order of 20 photospheric areas for both runs. The range scale on these plots gives the point of reflection in the corona, expressed in units of solar radii from the sun's center. An additional group delay of 2 sec is assumed (Chapter VI). This range scale will be used in all succeeding figures as well.

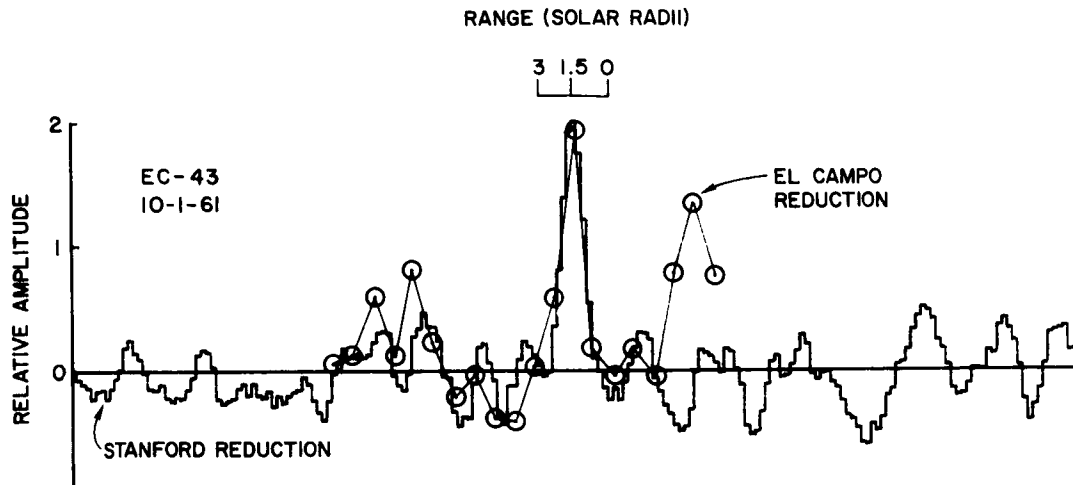


Fig. 15. CORRELATION OUTPUTS FROM EL CAMPO TAPE EC-43.

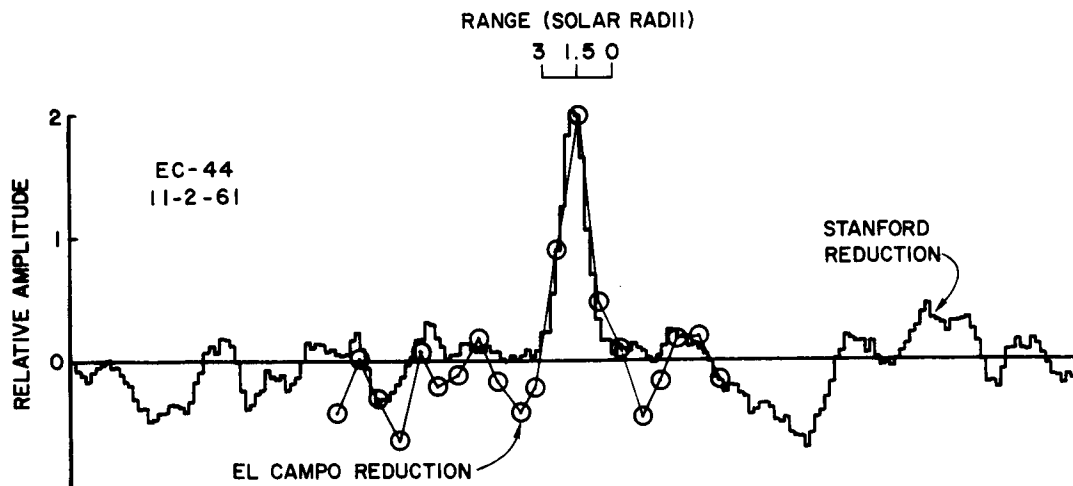


Fig. 16. CORRELATION OUTPUTS FROM EL CAMPO TAPE EC-44.

CHAPTER VI

EXPERIMENTAL RESULTS

Some specific details of the experimental work will now be discussed. These will include background noise, round-trip time calculations, calculation techniques for the measurements, and the procedure for summing many runs.

Since the background noise was almost entirely galactic, the effective temperature of the antenna was dependent only upon the region of the sky toward which it was pointed. Thus the background noise during transit varied only slowly from day to day. During the near-transit period the level would slowly change as the beam swept across the sky. The sky temperatures which were seen corresponded very well with what is expected by extending the radio sky map at 64 MHz [Hey et al, 1948] to 25 MHz with a spectral index of 2.6. The noise level was consistent enough to allow the use of calculated noise levels for computation, with accurate measurements of the noise level being made periodically to check on this assumption.

By knowledge of the noise level (with corrections for interference or solar noise bursts) and using the results of Chapter IV, the correlation output may be calibrated in terms of received signal power. By estimating the fraction (β) of the returned signal power that was accepted through the system's filters, compensating for the overlap of the signal channels, and using the radar equation, the output may be

calibrated directly in terms of radar cross section. The calculations of the overlap and the resultant value of β were made by assuming that the doppler spreading of the signal which was experienced at 38 MHz for 1963-1964 would be a reasonable estimate of the 25 MHz situation if it were scaled by the frequency ratio. Accordingly, Fig. 7 of James [1966] was scaled to produce Fig. 17. The choice of where to diminish the tails to zero is somewhat arbitrary since the data are not well established outside of the doppler spreading range

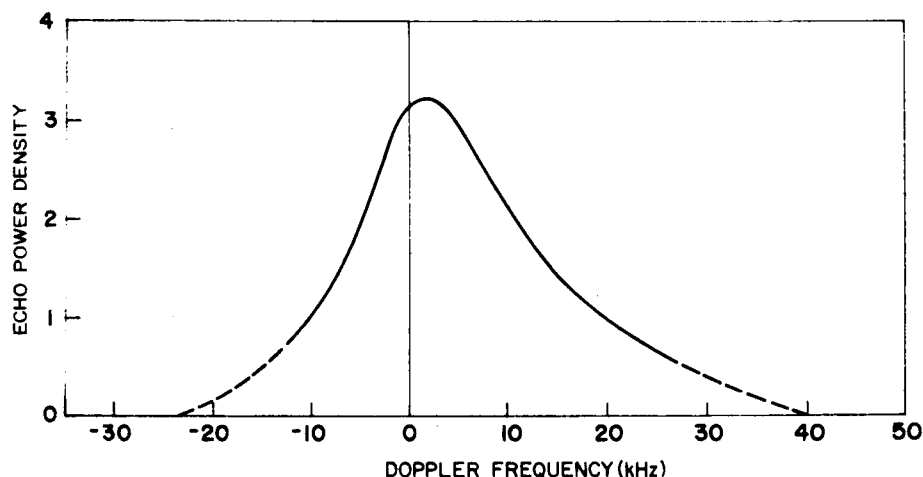


Fig. 17. ESTIMATED 25 MHz FREQUENCY SPREAD BASED UPON EL CAMPO RESULTS AT 38 MHz.

(on the present scale) of $(-12, +18)$ kHz. The integral of the product of this function and the system filter shape, with overlap included and using appropriate normalization, gives the estimate of the fraction of power actually accepted by the system. The 1963 system, due to the small frequency

shift (16 kHz) and the consequent large overlapping of the two channels, has an estimated value of β of 0.25; 1964 was much better due to a larger shift (40 kHz), giving 0.38. The 50 kHz shift used in 1965 gives an estimate for β of 0.42.

The calculation of round-trip times was made using 149,599,000 km for the astronomical unit (nominal earth-sun distance), 299,793 km/sec for the speed of light, 696,000 km for the photospheric radius, and 6378 km for the earth's radius. The standard ephemerides [American Ephemeris and Nautical Almanac, 1963, 1964, 1965] were consulted for daily tabulation of relative earth position and were interpolated for the true time of transit at Stanford's longitude. An additional delay of 2 sec was included to account for group delay in the corona. This figure has been calculated [James, 1966] by assuming the coronal electron distribution determined from optical considerations by Pottasch [1960]. This distribution has principal application to periods of sunspot minimum. Since our data were taken near a minimum (1964 was the null), this seems to be a reasonable figure.

Echoes at frequencies lower than 38 MHz will be reflected at points farther from the photosphere. Reconsideration of the 1959 Stanford results by including a 2 sec group delay and correcting the time calculations indicates that echoes were probably obtained from the region 2.2 to 2.4 solar radii from the sun's center. The time correction was necessary since the

two-way travel time for 1 A.U. was originally based upon early Venus radar results which were in error by about 1 sec. Because of the small number of runs in 1959, this range can only be expected to be a guide.

In the digital computer, all data were first cross-correlated just as they came from the previous steps of the reduction. However, in many cases, even with amplitude limiting of the analog signals, large digital values were produced by interference or solar bursts. If the disturbances were well balanced in the two channels, good cancellation generally occurred. However, often an imbalance existed due to a variable spectral characteristic of the noise. In these cases, very noisy crosscorrelations would exist with standard deviations of the output occasionally reaching two orders of magnitude greater than typical values. A selective procedure in the computer program was used to correct abnormally large values of the input data points and of the difference between the channels, and additionally, to correct the estimate of input noise power level. All correlation plots shown here have been corrected when needed.

In the 1963 and 1965 runs, no great problems arose. In 1964, however, a fairly serious problem arose in the form of a subtle mechanical oscillation in the tape recorder with a period of approximately 27 sec. The difficulty apparently manifested itself as a slight buckling of the tape which produced a small gain variation on one data channel. Upon

subtraction and crosscorrelation, a semiperiodic component was present in the output. The difficulty was not apparent until the test series was concluded and many runs had been summed, producing a summation with very large variance. An analysis showed that with small error, the small gain variation, if sinusoidal, would produce an additive sinusoidal component after channel subtraction. It was also concluded that filtering could probably remove most of the corruption. Accordingly, spectral analyses were made and a digital rejection filter was incorporated in the computer program. Instead of acting upon each set of data with a convolution operation, which is expensive when done for many runs, even with the fastest computers, it was shown that the filtering operation could equivalently be performed upon the sequence against which the data would be correlated. The data were grouped by the spectral characteristic of their corruption and the convolution was performed only once for each group. The filtering was quite successful in removing the bulk of the corruption. However, enough remained to badly taint the data and raise the sensitivity threshold. The effective attenuation of the desired signal was only a few percent. Thus the 1964 data are still completely valid in spite of their higher noise level.

In 1963, valid data were obtained from 61 runs during the period 29 June through 10 July, and 3 August through 30 August. The output correlation for a typical day is shown

in Fig. 18. The symbol σ_0 denotes the radar cross section in units of the photospheric disk area ($1.52 \times 10^{18} \text{ m}^2$).

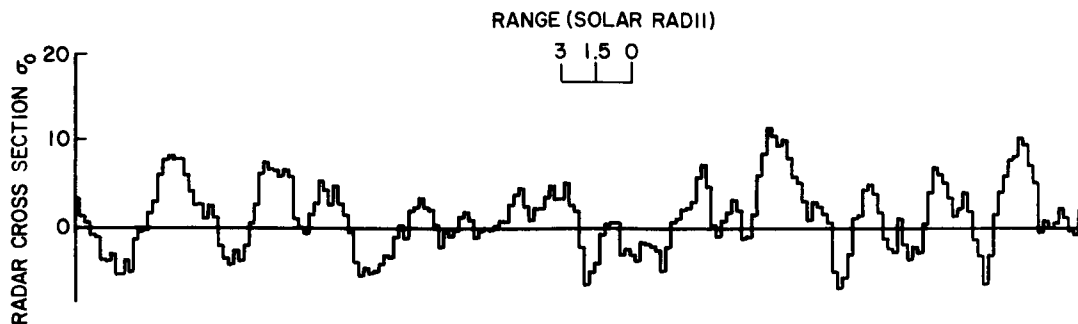


Fig. 18. TYPICAL 1963 CORRELATION OUTPUT - TAPE 283-2.

The 1963 runs generally had smaller fluctuations in the output since the two channels were much closer in frequency and better correlated. In none of the runs were echoes apparent.

The 1964 series consisted of 128 valid runs made in the period 2 July through 20 September. The output crosscorrelation for a typical run in this series is shown in Fig. 19. Again, no echoes were apparent in any of the runs.

The 1965 series was done between 31 August and 24 September with a total of 38 valid runs being made. A typical output correlation is shown in Fig. 20. No echoes were apparent in any of the runs.

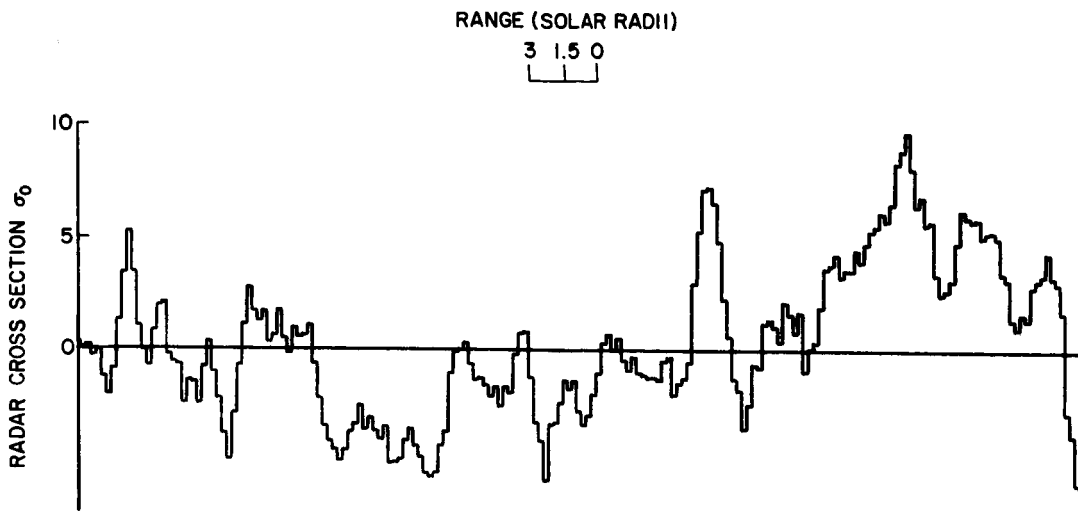


Fig. 19. TYPICAL 1964 CORRELATION OUTPUT - TAPE 499-1.

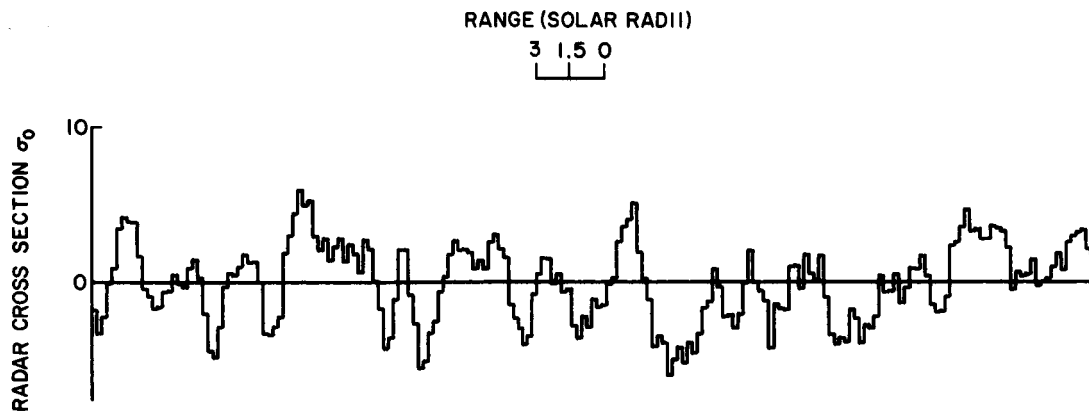


Fig. 20. TYPICAL 1965 CORRELATION OUTPUT - TAPE 595-1.

A. Weighted Summations of Data Runs

A description will now be given of the technique used for summing many runs to improve the system's effective signal-to-noise ratio. A necessary first assumption is that the depth of penetration of the signal into the corona is reasonably constant with time so that a composite echo may be built up by shifting each individual output to correct for changes in round-trip time caused by the changing earth-sun distance. By calculations, then, we may determine a value of α_i and t_i for each run such that the i^{th} output can be expressed as

$$c_j^{(i)} = \alpha_i \sigma_0 \rho_{j-t_i} + N_j^{(i)} \quad (59)$$

where $c_j^{(i)}$ is the j^{th} point of the correlation for a run indexed by i , α_i incorporates all the system parameters in the radar equation, σ_0 is the radar cross section of the sun in photospheric area units and is assumed to be constant for all runs that will be summed, ρ_{j-t_i} denotes the autocorrelation function of the signal shifted by a relative delay t_i , and $N_j^{(i)}$ is the (zero-mean) noise at output point j of the i^{th} run.

A linear weighting is proposed:

$$\hat{c}_j = \sum_{i=1}^M \beta_i c_{j+t_i}^{(i)} \quad (60)$$

where \hat{C}_j is the summed output and β_i is a weighting factor for the i^{th} run. $C_j^{(i)}$ is shifted by t_i so that all echo peaks are brought into coincidence. An optimum set of weightings exists; and by a simple argument, using the Cauchy-Schwarz inequality, the optimum β_i 's which give the maximum signal-to-noise ratio for \hat{C}_j are found to be [Brennan, 1959]

$$\beta_i = (\text{const}) \frac{\alpha_i}{E\left\{\left[N_j^{(i)}\right]^2\right\}} \quad (61)$$

By proper choice of this constant, \hat{C}_j becomes an unbiased, consistent estimator of σ_0 . Since the signal peak is weaker than the noise,

$$E\left\{\left[N_j^{(i)}\right]^2\right\} \cong E\left\{\left[C_j^{(i)}\right]^2\right\} \quad (62)$$

All parameters are thus determined for optimum weighting. The expectation of Eq. (62) can be approximated very well by a simple summation if the average of $C_j^{(i)}$ is near zero. To ensure that a drift in $C_j^{(i)}$ will not cause a large inverse weighting for an individual run, a linear curve is fitted to each output in the minimum mean-square-error sense. After this curve is subtracted, the calculation of noise variance is made and the summation is performed.

This technique was used to perform 64 different data summations, with various criteria used to select the groups

to be summed. Groupings were made by means of year, general noisiness, specific noise due to solar activity, high and low sunspot numbers, and several combinations of the above. No echoes were apparent in any of these summations. The significant summations are shown in Figs. 21 to 24. The total summation for each year is given, as well as the sum of all 3 years.

One additional set of 12 summations was performed incorporating the actual daily cross-section values measured at El Campo on the days that both systems were run [James, 1967]. These values were used as an additional multiplicative factor. The plotting scale is thus the average fraction of the El Campo values seen by the Stanford system. For 1963, 28 runs were coincident and were summed; for 1964, 62 runs; for 1965, 32 runs. The results are shown in Figs. 25 to 27. In addition, all runs of this category were summed for all 3 years and the result appears in Fig. 28. Figure 25 presents the only summation of any large number of runs which could represent a returned signal. If this were the case, it would mean that the average fraction of the El Campo cross section represented by these data would be 0.85. This is certainly not an unreasonable value. However, the significance of this peak is very low (2.5 standard deviations above the rest of the output) and consequently nothing can be reasonably claimed.

Since echoes were not readily apparent in any of the

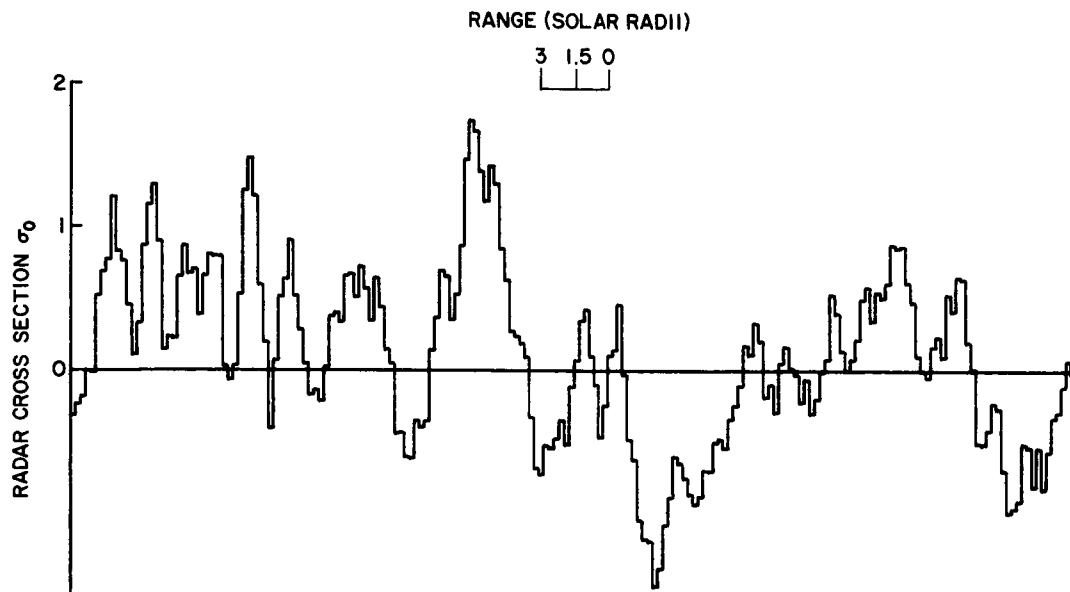


Fig. 21. 1963 SUMMATION OF 61 RUNS.

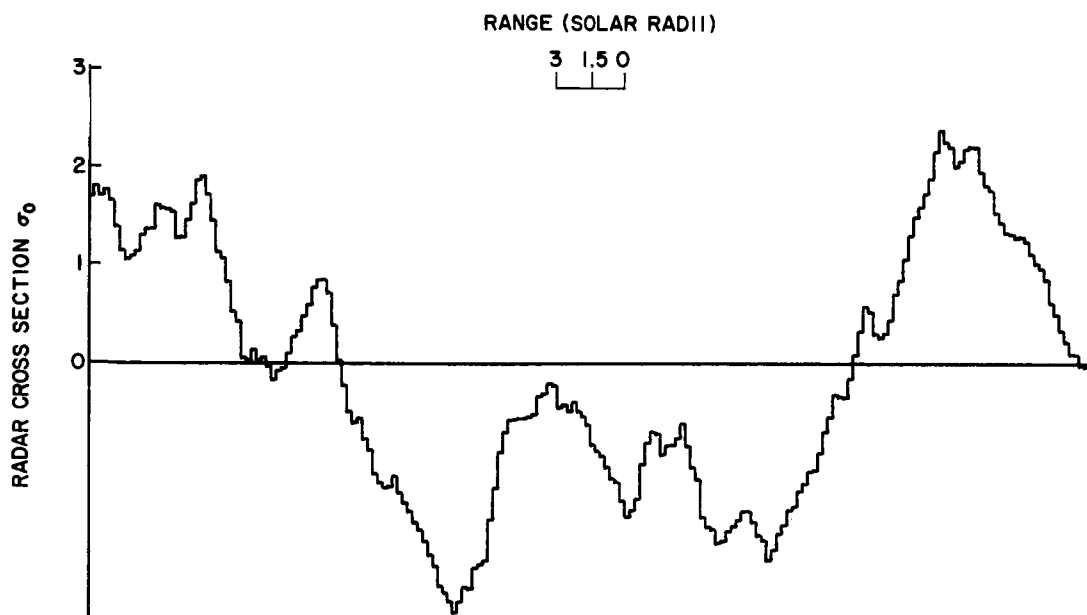


Fig. 22. 1964 SUMMATION OF 128 RUNS.

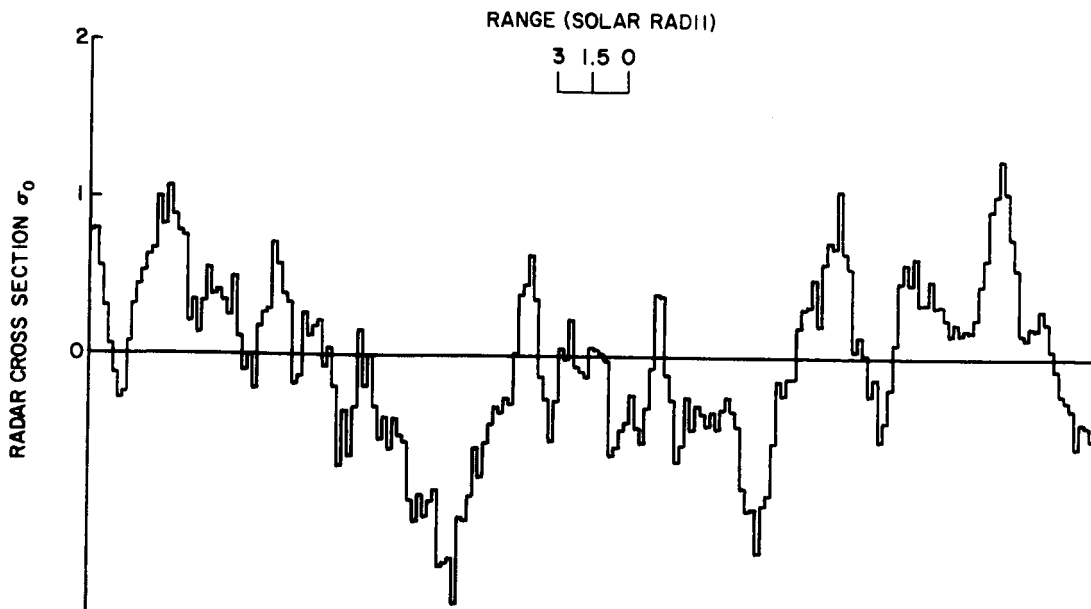


Fig. 23. 1965 SUMMATION OF 38 RUNS.

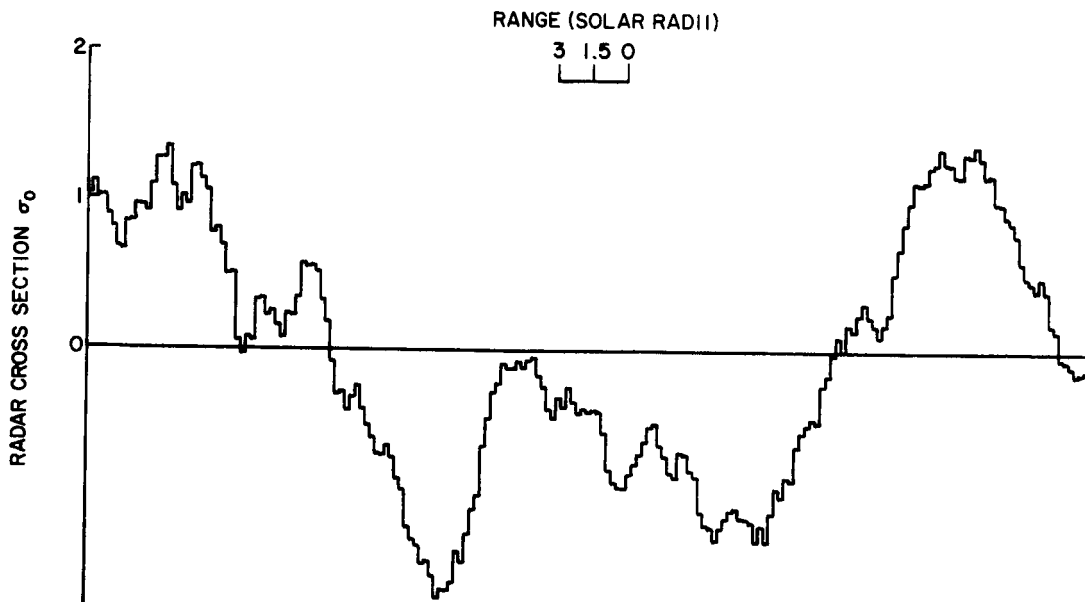


Fig. 24. TOTAL SUMMATION OF 227 RUNS.

data summations, it would seem reasonable to consider Figs. 21 through 23 as providing the most realistic assessment of the situation, since the summations in these figures include all the runs for each year. If the cross section were large enough to produce a substantial peak, then an estimate of the average cross section during the runs of each year would be obtained. If a peak is not apparent, then an upper bound on the average radar cross section may be estimated if it is known that the returned signal did exist in the system but was below the detection threshold. It is impossible to prove that a signal existed if it could not be detected. The best that can be done is to show a high probability of existence. It is claimed that this has been demonstrated in Chapter V. The principal reason for the delay before reporting these results was to permit substantiation of this claim. Accepting this claim, we may estimate the magnitude of cross section which would be readily detectable. Since we are looking for a peak with the shape of Fig. 6 within a few solar radii of the sun, a maximum value of 2 for the average cross section of each year's data is quite conservative, especially for 1964 (Fig. 22) and 1965 (Fig. 23). A peak of this magnitude would be readily apparent in all three plots. In addition, Fig. 24 shows that this value is reasonable when considering the average of all 227 runs.

The conservative conclusion for the data is that the average radar cross section of the sun was below two

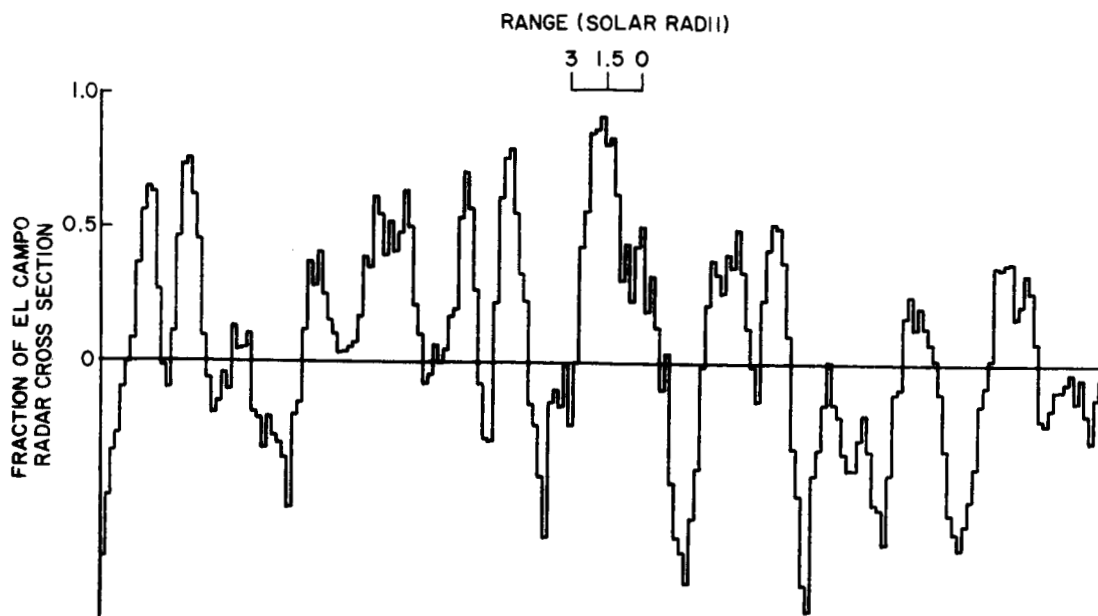


Fig. 25. EL CAMPO WEIGHTING AND SUMMATION OF 28 RUNS FROM 1963.

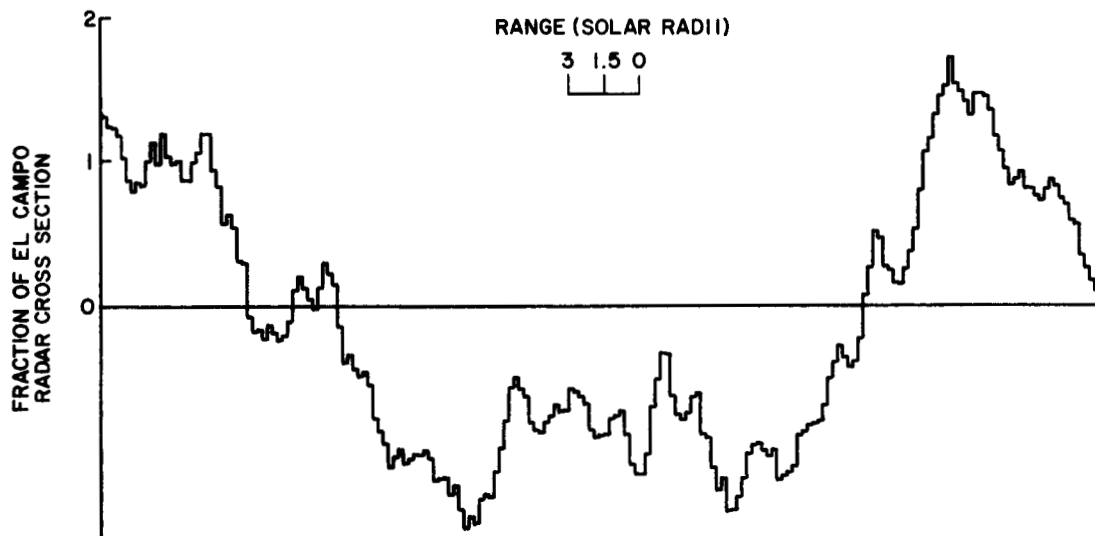


Fig. 26. EL CAMPO WEIGHTING AND SUMMATION OF 62 RUNS FROM 1964.

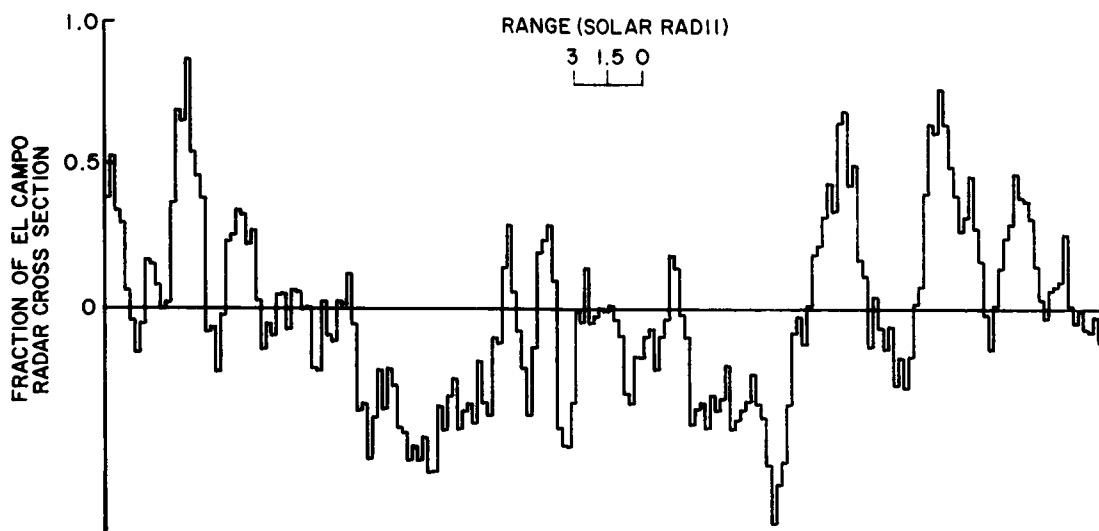


Fig. 27. EL CAMPO WEIGHTING AND SUMMATION OF 32 RUNS FROM 1965.

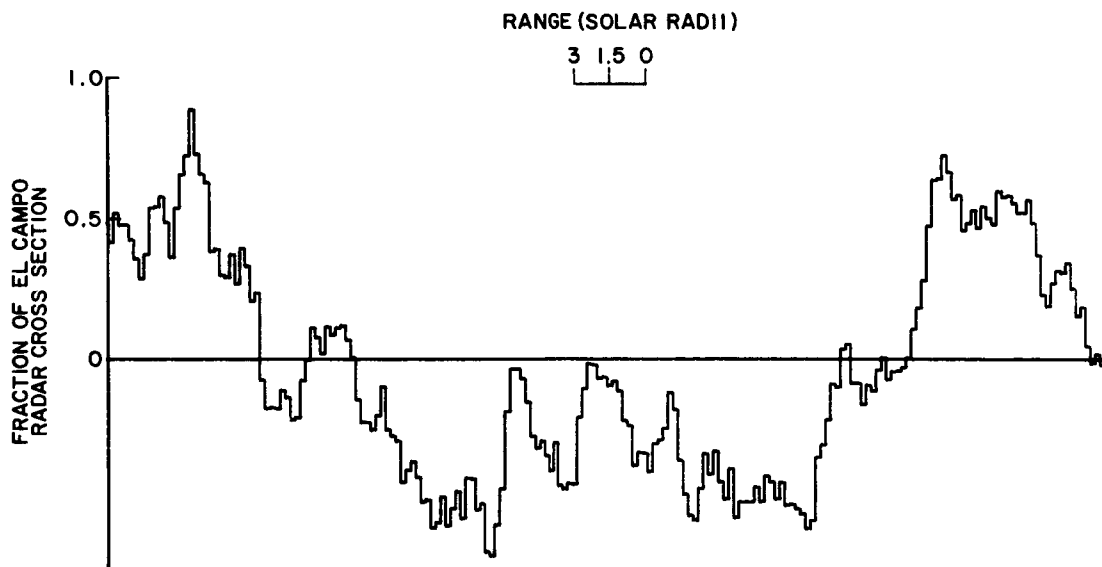


Fig. 28. EL CAMPO WEIGHTING AND SUMMATION OF 122 RUNS FOR 1963, 1964, 1965.

photospheric disk areas during the investigation periods of all 3 years.

B. Comparison with Other Experiments

In Fig. 29 are shown the average results of the six successful Stanford experiments of April and September 1959, and the M.I.T. measurements, which have been nearly continuous since 1961. After James [1964], the original Stanford results, which used only a 2 kHz bandwidth, have been corrected to apply for the total energy which would be received in a very wide bandwidth. This is done by scaling the 38 MHz frequency spreading (echo spectrum) to 26 MHz (as in Fig. 17) and comparing total powers. The value of 80 which is obtained for σ_0 is probably a minimum value due to the conservative values used for some of the system parameters. The average cross section values for 2 to 3 month periods are shown for the El Campo data [James, 1966]. The unusually large individual values of σ_0 were not included in the monthly means [James, 1967]. The yearly average (Zurich) sunspot number is also displayed. The long-term correlation of the measured El Campo values and the sunspot number is quite apparent. The maximum value of $\sigma_0 = 2$ at 25 MHz represents the sensitivity of the Stanford system as discussed previously.

The first point to consider is the large decrease in σ_0 between 1959 and 1963-1965 at 25 MHz. The small frequency difference between the two sets of experiments at Stanford

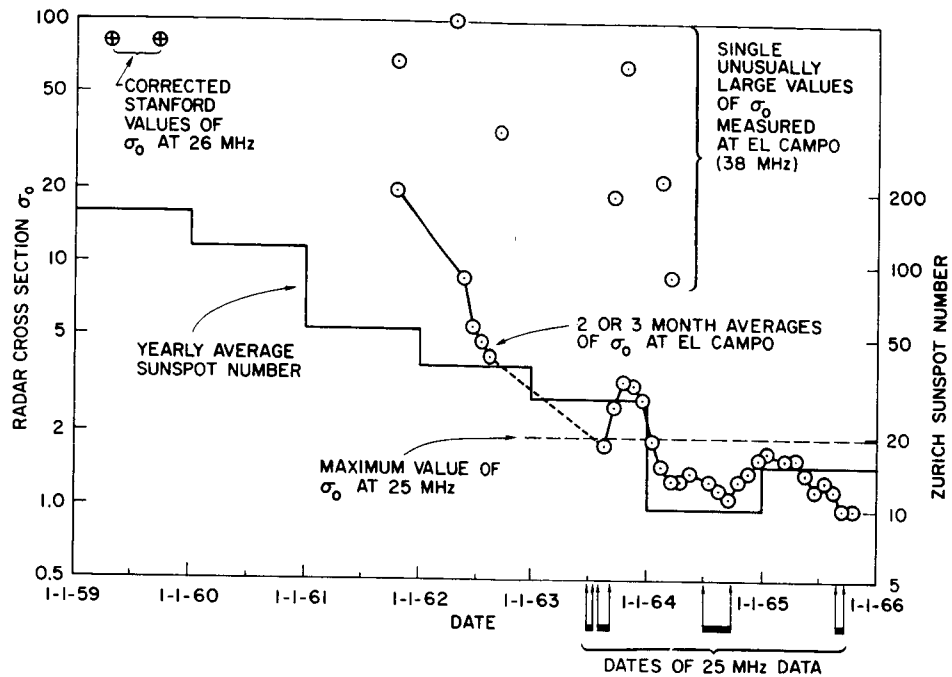


Fig. 29. COMPARISON OF RADAR CROSS SECTION MEASUREMENTS.

(about 1 MHz) could not be responsible. The general level of solar activity is indexed quite well by the sunspot number. Thus a high sunspot number could reasonably be expected to be correlated with a more active and disturbed coronal region, which could then produce a larger number of regions with reflecting surfaces capable of directing energy back to earth. Thus it would seem reasonable that high values of cross section could occur during years of high sunspot number, whereas when the sun was relatively stable during sunspot minima, the cross section would be lower. This correlation with the sunspot cycle appears to be a reasonable explanation for the observed variation in σ_0 . There is the possibility that the

1959 measurements arose from the same phenomenon which produced the unusually large values of σ_0 at 38 MHz. Whatever this phenomenon is, it may be very common near sunspot maximum. It certainly does not seem to be common during the minimum of the sunspot cycle. In any event, the 1959 results were obtained on 5 separate days in two groups 5 months apart. The signal levels received, while certainly not identical, were consistent enough to indicate that they were probably typical of the sun's behavior during this entire period.

The claimed correlation of sunspot number and σ_0 becomes more reasonable when the 38 MHz data are considered as well. The El Campo values exhibit a definite correlation with the yearly sunspot average. However, on a daily basis the correlation is very low [James, 1966].

Theoretical consideration [Yoh, 1961] of the corona as a radar reflector indicates that lower frequencies should experience a larger cross section because of less attenuation due to the signal being reflected from higher in the corona. The present results, however, show that the 25 MHz cross section could not be much greater than that at 38 MHz or detection certainly would have occurred. It should be observed from Fig. 29, however, that each of the 1963-1965 series of runs coincided with very small values of σ_0 at 38 MHz.

CHAPTER VII

CONCLUSIONS

A. Summary and Conclusions

A model for a radar system to detect the sun has been established and investigated. The conditions for maximum signal detectability were derived and discussed.

A model of the time-varying reflectivity of the corona is developed in terms of its effect upon measurement of the average reflectivity (i.e., radar cross section). This is incorporated into an overall model of the fluctuating signal problem which includes the effect of random signal polarization changes due to Faraday rotation in the ionosphere and/or corona. The net effect upon measurement is shown to be well represented by considering a "slow" or "fast" fading model.

The results of the experimental work, while negative, nevertheless imply interesting positive conclusions, due to a demonstration of the radar system's validity. The average radar cross section of the sun is shown to be less than two units of photospheric disk area for each of the 3 years the experiments were performed.

When compared with the 1959 Stanford results, a correlation with the sunspot cycle is implied for the radar cross section. While this conclusion is weak by itself, the general large decrease of cross section with decrease in sunspot number observed by M.I.T. lends weight to this argument. The results indicate, in addition, that the radar cross section

of the sun at 25 MHz is probably not significantly greater than at 38 MHz, if as large at all.

B. Suggestions for Future Work

The dynamic nature of the sun and the remarkable variation of its radar characteristics with time certainly make it desirable that further investigations be carried out. A more sensitive system is required than that at Stanford if low-frequency investigations are desired during periods of low solar activity. However, if the cross section is high every 11 years, then during this period systems comparable to Stanford's sensitivity probably will be able to obtain echoes. It should be realized, though, that the last sunspot maximum of 1956-1960 was the largest ever observed.

The complexity of the corona makes it desirable that every tool of the radar astronomer be applied in order to evaluate the sun's behavior. The variation of radar cross section with time and frequency, and the spectrum and time spread of the reflected signal are obviously desirable quantities for measurement. Moreover, simultaneous measurement of these quantities at various frequencies would be very valuable since it would give the state of the corona at various depths at the same time. A system (or combination of systems) which could investigate the corona at two greatly differing frequencies simultaneously or could alternately transmit a minute or two at each, would give very valuable results.

It would also be valuable if the short-term polarization effects of the corona could be determined. Unfortunately, the effect of the ionosphere must be removed. Signals of various polarizations (i.e., linear and circular) should be transmitted and then received by means of variously polarized antennas. Measurements of the ionospheric effects by using the moon or a satellite as a reference would allow determination of the corona's effects. This could be expected to give some information on the sun's magnetic field.

Resolution of all coronal radar parameters within short time intervals is very desirable but requires correspondingly greater sensitivity.

APPENDIX
SIGNAL PROCESSOR ANALYSIS

The receiver model of Fig. 7 is analyzed in this appendix under the major assumptions of negligible time spread, negligible fading, random carriers, and other minor assumptions of Chapter IV.

Just after the bandpass filter $H_1(f)$, $x(t)$ is given by

$$x(t) = K_1 [h_1(t) * r(t)] \quad (A-1)$$

where $*$ denotes convolution and $h_1(t)$ is the impulse response of filter $H_1(f)$. Since s_1 and s_2 are slow compared to $g_1(t)$,

$$x(t) = K_1 \left\{ \sqrt{R} s_1(t) [g_1(t) * h_1(t)] + \sqrt{R} s_2(t) [g_2(t) * h_1(t)] + [n(t) * h_1(t)] \right\} \quad (A-2)$$

For convenience, $t = 0$ is considered to be coincident with the leading edge of the returned signal. The middle term of (A-2) is zero since $G_2(f)$ and $H_1(f)$ are disjoint.

Thus

$$x(t) = K_1 [\sqrt{R} s_1(t) g_1'(t) + n_1(t)] \quad (A-3)$$

where

$$g_1'(t) = g_1(t) * h_1(t) \quad (A-4)$$

$$n_1(t) = n(t) * h_1(t) \quad (A-5)$$

The power spectra for $g_1'(t)$ and $n_1(t)$, which are stationary gaussian random processes, are

$$G_1'(f) = G_1(f) |H_1(f)|^2 \quad (A-6)$$

$$N_1(f) = |H_1(f)|^2 N(f) = |H_1(f)|^2 \frac{N_0}{2} \quad (A-7)$$

Now x_k is given by

$$\begin{aligned} x_k &= \int_{k-1}^k x^2(t) dt \\ &= K_1^2 \int_{k-1}^k \left\{ R s_1^2(t) [g_1'(t)]^2 + n_1^2(t) \right. \\ &\quad \left. + 2\sqrt{R} s_1(t) g_1'(t) n_1(t) \right\} dt \end{aligned} \quad (A-8)$$

Since g_1 and n are zero mean, then g_1' and n_1 are zero mean and

$$E[x_k] = K_1^2 \int_{k-1}^k R \left\{ s_1^2(t) E[g_1'^2(t)] + E[n_1^2(t)] \right\} dt \quad (A-9)$$

Now

$$E[n_1^2(t)] = \int_{-\infty}^{\infty} N_1(f) df = \frac{N_0}{2} \int_{-\infty}^{\infty} |H_1(f)|^2 df \quad (A-10)$$

and

$$E[g_1'^2(t)] = \int_{-\infty}^{\infty} G_1(f) |H_1(f)|^2 df \quad (A-11)$$

Thus

$$E[x_k] = K_1^2 \left[\int_{-\infty}^{\infty} G_1(f) |H_1(f)|^2 df \right] R \int_{k-1}^k s_1^2(t) dt + K_1^2 \frac{N_0}{2} \int_{-\infty}^{\infty} |H_1(f)|^2 df \quad (A-12)$$

Since $|H_1(f)| \leq 1$ and the integral of $G_1(f)$ is unity, β may be defined as that fraction of the returned signal power around frequency f_1 that gets through the filter $H_1(f)$. Thus

$$1 \geq \beta \triangleq \int_{-\infty}^{\infty} G_1(f) |H_1(f)|^2 df \quad (A-13)$$

Using the definition of noise bandwidth W from Eq. (12), we obtain

$$E[x_k] = K_1^2 \beta R \int_{k-1}^k s_1^2(t) dt + K_1^2 N_0 W \quad (A-14)$$

The quantity \bar{x} is the average of the x_k defined as

$$\bar{x} = \frac{1}{1000} \sum_{k=1}^{1000} x_k \quad (A-15)$$

From Eq. (A-14) it is seen that

$$E[\bar{x}] = \frac{K_1^2 \beta R}{1000} \int_0^{1000} s_1^2(t) dt + K_1^2 N_0 W \quad (A-16)$$

Since $s_1(t)$ is 0 or 1 alternately, with an average value of about one-half, the first term is about $(1/2) K_1^2 \beta R$. Also

this gives $s_1^2(t) = s_1(t)$. Now, since the ratio of signal power (βR) to noise power ($N_0 W$) is much less than unity, the first term is negligible. Hence $E[\bar{x}] = K_1^2 N_0 W$. The variance of \bar{x} is 1/1000 of the variance of x_k , thus we may make the approximation

$$\bar{x} \approx K_1^2 N_0 W \quad (\text{A-17})$$

Thus

$$x'_k = \frac{x_k}{\bar{x}} \quad (\text{A-18})$$

and

$$E[x'_k] = \frac{\beta R}{N_0 W} \int_{k-1}^k s_1(t) dt + 1 \quad (\text{A-19})$$

Similarly for the other channel,

$$E[y'_k] = \frac{\beta R}{N_0 W} \int_{k-1}^k s_2(t) dt + 1 \quad (\text{A-20})$$

Thus the expected difference signal d_k is

$$E[d_k] = E[x'_k - y'_k] = \frac{\beta R}{N_0 W} \int_{k-1}^k [s_1(t) - s_2(t)] dt \quad (\text{A-21})$$

From the encoding scheme [Eq. (7)] the integrand is seen to be the transmit sequence $s(t)$. Since s_k is $s(t)$ for $t \in (k-1, k)$, we have

$$E[d_k] = \frac{\beta R}{N_0 W} s_k \quad (\text{A-22})$$

The crosscorrelation producing C_j is

$$C_j = \sum_{k=1}^{1000} d_k s_{k-j} \quad (\text{A-23})$$

Therefore

$$E[C_j] = \frac{\beta R}{N_o W} \sum_{k=1}^{1000} s_k s_{k-j} \quad (\text{A-24})$$

From Eq. (5), the summation is simply $10^3 \rho_j$.

Thus

$$E[C_j] = 10^3 \frac{\beta R}{N_o W} \rho_j \quad (\text{A-25})$$

The crosscorrelation output thus consists of a copy of the signal autocorrelation with an amplitude proportional to the input signal-to-noise ratio. When the time origin of the processing is not coincident with the signal's return, the relative delay produces a shift in the position of the autocorrelation "copy" in the output. A relative delay which is not an integral number of seconds will also cause a small distortion of the apparent copy due to the sampling of the true autocorrelation function. Thus, when the sampling rate and signal have noninteger relative delay, a sample will not occur at the actual peak of the true autocorrelation. The two resulting highest samples will, however, both be larger than the normal second highest in value. For a returned signal with a large SNR and no time spreading, the exact arrival time can be determined by a simple analysis of the

distortion in shape. This is done by a simple extrapolation of the points comprising the sides of the central peak. In practice, however, time spread and noise generally preclude an analysis of this accuracy for an individual run.

Thus if round-trip time were T_R and the processor's time origin were T_0 with respect to transmit beginning, then

$$E[C_j] = 10^3 \frac{BR}{N_0 W} \rho_{j-(T_R-T_0)} \quad (A-26)$$

The output variance will now be determined. With reference to Eq. (A-8),

$$E[x_k^2] = E \int_{k-1}^k \int_{k-1}^k x^2(t) x^2(\tau) dt d\tau \quad (A-27)$$

Because of the low SNR assumption, the only portion of $x(t)$ from (A-3) which is significant for this analysis is $K_1 n_1(t)$. Thus

$$E[x_k^2] = K_1^4 \int_{k-1}^k \int_{k-1}^k E[n_1^2(t) n_1^2(\tau)] dt d\tau \quad (A-28)$$

Since $n_1(t)$ is zero mean and gaussian we may use the relation

$$E[ABCD] = E[AB] E[CD] + E[AC] E[BD] + E[AD] E[BC] \quad (A-29)$$

where A, B, C, D are zero-mean gaussian random variables [Wainstein and Zubakov, 1962]. Thus

$$E[x_k^2] = K_1^4 \left\{ E^2[n_1^2(t)] + 2 \int_{k-1}^k \int_{k-1}^k E^2[n_1(t) n_1(\tau)] dt d\tau \right\} \quad (\text{A-30})$$

The autocorrelation function of $n_1(t)$ is defined as

$$R_{n_1}(t-\tau) = E[n_1(t) n_1(\tau)] \quad (\text{A-31})$$

Thus

$$E[x_k^2] = K_1^4 E^2[n_1^2(t)] + 2K_1^4 \int_{k-1}^k \int_{k-1}^k R_{n_1}^2(t-\tau) dt d\tau \quad (\text{A-32})$$

Since the signal is assumed negligible in the present computation, it is seen from Eq. (A-9) that

$$E[x_k] = E[n_1^2(t)] K_1^2 \quad (\text{A-33})$$

Therefore, the variance of x_k is given by

$$\text{Var}[x_k] = E[x_k^2] - E^2[x_k] = 2K_1^4 \int_{k-1}^k \int_{k-1}^k R_{n_1}^2(t-\tau) dt d\tau \quad (\text{A-34})$$

By a change of variable, $\xi = t-\tau$,

$$\text{Var}[x_k] = 2K_1^4 \int_{k-1}^k \int_{k-1-\tau}^{k-\tau} R_{n_1}^2(\xi) d\xi d\tau \quad (\text{A-35})$$

Since the bandwidth of $n(t)$ is generally at least a few kilohertz, $R_{n_1}(\xi)$ will fall to zero for values of ξ much

smaller than the inner integral limits. Thus the error in changing those limits to $\pm\infty$ is negligible. Thus

$$\text{Var}[x_k] = 2K_1^4 \int_{-\infty}^{\infty} R_{n_1}^2(\xi) d\xi \quad (\text{A-36})$$

Since $R_{n_1}(\xi)$ and $N_1(f)$ form a Fourier transform pair, we may apply Parseval's theorem and write

$$\begin{aligned} \text{Var}[x_k] &= 2K_1^4 \int_{-\infty}^{\infty} N_1^2(f) df \\ &= 2K_1^4 \int_{-\infty}^{\infty} |H_1(f)|^4 \frac{N_0^2}{4} df \\ &= \frac{K_1^4 N_0^2}{2} \int_{-\infty}^{\infty} |H_1(f)|^4 df \end{aligned} \quad (\text{A-37})$$

Since x'_k and x_k are related by a constant [Eqs. (A-17), (A-18)],

$$\text{Var}[x'_k] = \frac{1}{\bar{x}^2} \text{Var}[x_k] = \frac{1}{2W^2} \int_{-\infty}^{\infty} |H_1(f)|^4 df \quad (\text{A-38})$$

Since x_k and y_k are independent but statistically identical,

$$\begin{aligned} \text{Var}[d_k] &= \text{Var}[x'_k] + \text{Var}[y'_k] \\ &= \frac{1}{W^2} \int_{-\infty}^{\infty} |H(f)|^4 df \end{aligned} \quad (\text{A-39})$$

If we wish to consider only the noisy portion of the cross-correlation output, we begin with

$$\text{Var}[C_j] = E[C_j^2] - E^2[C_j] \quad (\text{A-40})$$

The last term will be effectively removed if we consider only the variance of the input to the correlator (i.e., ignore the signal component of d_k). Using Eq. (A-23),

$$\begin{aligned} \text{Var}[C_j] &= E \left[\sum_{k=1}^{1000} d_k s_{k-j} \right]^2 \\ &= \sum_{k=1}^{1000} \sum_{n=1}^{1000} E[d_k d_n] s_{k-j} s_{n-j} \quad (\text{A-41}) \end{aligned}$$

Successive values of d_k are independent when the signal is ignored, thus

$$E[d_k d_n] = \begin{cases} \text{Var}[d_k] & k = n \\ 0 & k \neq n \end{cases} \quad (\text{A-42})$$

Therefore

$$\text{Var}[C_j] = \sum_{k=1}^{1000} \text{Var}[d_k] s_{k-j}^2 \quad (\text{A-43})$$

Since s_k is ± 1 , its square is unity, and using Eq. (A-39) we obtain

$$\text{Var}[C_j] = \frac{10^3}{W^2} \int_{-\infty}^{\infty} |H(f)|^4 df \quad (\text{A-44})$$

The noise component of C_j which causes this variance essentially arises from the sum of a large number of independent random variables. This number is the number of degrees of freedom of the noise and is twice the time-bandwidth product. The total bandwidth can be considered to be $2W$ for the two channels. Therefore, for a 10 kHz bandwidth and a 1000 sec signal interval, the number of degrees of freedom would be 4×10^7 . From the Central Limit Theorem [Davenport and Root], it can be reasonably expected that the noise component of C_j will exhibit a gaussian distribution. This can be expected to be true for any stationary input noise regardless of its actual distribution.

BIBLIOGRAPHY

- Abel, W. G., et al, "Radar Reflections from the Sun at Very High Frequencies," J. Geophys. Res., 66, 12, Dec 1961, pp. 4303-07.
- Abel, W. G., et al, "A V.H.F. Solar Radar System," IRE Intern. Conv. Record, 10, Pt. 5, 1962, pp. 58-66.
- American Ephemeris and Nautical Almanac, U.S. Naval Observatory, 1963, 1964, 1965.
- Barthle, R. C., "The Detection of Radar Echoes from the Sun," Report AFCRL-TN-60-969, Scientific Report No. 9, Contract AF 19(604)-2193, Stanford Electronics Laboratories, Stanford, Calif., 24 Aug 1960.
- Bass, F. G., and S. Ia. Braude, "On the Questions of Reflecting Radar Signals from the Sun," Ukrainian J. Phys., 2, 2, 1957, pp. 149-64.
- Brennan, D. G., "Linear Diversity Combining Techniques," Proc. IRE, 47, Jun 1959, pp. 1075-1102.
- Chisholm, J. H., and J. C. James, "Radar Evidence of Solar Wind and Coronal Mass Motions," Astrophys. J., 140, Jul 1964, pp. 377-79.
- Davenport, W. B., Jr., and W. L. Root, An Introduction to the Theory of Random Signals and Noise, McGraw-Hill Book Company, New York, 1958.
- Dyce, R. B., private communication, 1967.
- Eshleman, V. R., R. C. Barthle, and P. B. Gallagher, "Radar Echoes from the Sun," Science, 131, 3397, Feb 1960, pp. 329-332.
- Golomb, S. W., (Ed.), Digital Communications with Space Application, Prentice-Hall, Inc., Englewood Cliffs, N.J., 1964.
- Green, P. E., Jr., "Radar Astronomy Measurement Techniques," Technical Report No. 282, Lincoln Laboratory, M.I.T., 1962.
- Hey, J. S., S. J. Parsons, and J. W. Phillips, "An Investigation of Galactic Radiation in the Radio Spectrum," Proc. Roy. Soc. A., 192, 1948, pp. 425-445. Alternatively see H. C. Ko, "The Distribution of Cosmic Radio Background Radiation," Proc. IRE, Jan 1958, pp. 208-215.

- Howard, H. T., "An Antenna Array for Radar Astronomy Studies in the 20 to 55 Mc Range," IEEE Trans. on Antennas and Propagation, AP-13, May 1965, pp. 365-368.
- James, J. C., "Radar Echoes from the Sun," IEEE Trans. on Military Electronics, MIL-8, Jul-Oct 1964, pp. 210-225. Also published in IEEE Trans. on Antennas and Propagation, AP-12, Dec 1964, pp. 876-91.
- James, J. C., "Radar Studies of the Sun at 38 Mc/s," Astrophys. J., 146, 2, Nov 1966, pp. 356-366.
- James, J. C., private communication, 1967.
- Kerr, F. J., "On the Possibility of Obtaining Radar Echoes from the Sun and Planets," Proc. IRE, 40, 6, Jun 1952, pp. 660-666.
- Klemperer, W. K., private communication, 1967.
- Parzen, E., Modern Probability Theory and Its Applications, John Wiley & Sons, Inc., New York, 1960.
- Pottasch, S. R., "Use of the Equation of Hydrostatic Equilibrium in Determining the Temperature Distribution in the Outer Solar Atmosphere," Astrophys. J., 131, 1960, pp. 68-74.
- Stanford Radioscience Laboratory (lunar radar papers):
Howard H. T., P. Yoh, and V. R. Eshleman, "Radar Doppler Measurements of the Cislunar Medium," J. Geophys. Res., 69, 3, 1 Feb 1964, pp. 535-539.
- Howard, H. T., et al, "Radar Measurements of the Cislunar Electron Content," J. Geophys. Res., 70, 17, 1 Sep 1965, pp. 4357-63.
- Howard, H. T., et al, "Radar Doppler and Faraday Polarization Measurements of the Cislunar Medium during the July 20, 1963 Solar Eclipse," J. Geophys. Res., 69, 3, 1 Feb 1964, pp. 540-544.
- Yoh, P., et al, "Lunar Radar Measurements of the Earth's Magnetospheric Wake," J. Geophys. Res., 71, 1, 1 Jan 1966, pp. 189-193.
- Wainstein, L. A., and V. D. Zubakov, Extraction of Signals from Noise, Prentice-Hall, Inc., Englewood Cliffs, N.J., 1962.

Yoh, P., "Calculations of Signal-to-Noise Ratios for Solar Radar Echoes," Report AFCRL-739, Scientific Report No. 2, Contract AF 19(604)-7436, Stanford Electronics Laboratories, Stanford, Calif., 18 Jul 1961.